NTNU – Trondheim
Norwegian University of
Science and Technology

Particle Mobility in Mucus

Role of Surface Interactions and Use of
G-blocks

Kari Jyssum

Biotechnology (5 year)

Supervisor: Kurt Ingar Draget, IBT

Norwegian University of Science and Technology
Department of Biotechnology

Preface

This thesis is a master's thesis conducted at the Norwegian University of Science and Technology, Institute of Biotechnology, October 2011-May 2012. The master's thesis is the final assignment in a five years long study program. The work was conducted in collaboration with the research group of Professor Kurt Ingar Draget, and with Catherine Taylor Nordgård as supervisor. The work has been challenging and at times frustrating, but also very interesting. I feel that I have learned a lot about research and how to proceed from one obstacle to the next without losing faith in my project. For this I would like to thank Catherine for her motivating enthusiasm, which is infectious, but also for helpful thoughts and remarks throughout the work. I would also like to thank Prof. Draget, Magnus and Julie for help and a very nice working environment in the lab, and Astrid Bjørkøy for help with Matlab coding and education on the confocal.

Last but not least I would like to thank my friends and fellow students, without whom these five years would not have been this livable. The comfort found in all our discussions and shearing of frustrations and joys is something I appreciate immensely. I also thank my family and Ola for never-ending support and motivation.

NTNU, Trondheim
May, 2012

_____

Kari Jyssum

Abstract

The mucus layers on the internal surfaces of the human body serve as an important barrier against foreign material, but it also create restrictions regarding drug delivery. Discovering methods to overcome this barrier would lead us closer to an efficient delivery of larger drugs and nanoparticles. Recent studies have shown that alginate G-block polymers can modify the physical properties of mucus, and that the G-blocks make the mucin network more open and increase particle transport through mucus. This shows that G-blocks are an interesting candidate, for use in drug delivery across mucosal barriers, but further work to understand the mechanisms by which the G-blocks interact with mucus is still desirable.

Studies have shown that neutral particles diffuse more easily through mucus than charged particles. In this thesis the interactions between nanoparticles with different surface structures and mucus components were compared by dynamic light scattering and the effect of G-block on these interactions was established. The diffusions of all particle types were compared in pig gastric mucin (PGM) from Sigma, by the use of confocal microscopy and multiple particle tracking (MPT). Then alginate G-blocks were added and the diffusion of the particle types was compared.

The results showed that G-blocks can reduce the amount of mucin components accumulating on to positively charged particles but not to negatively charged particles. The MPT showed that the surface charge of the nanoparticles is the primary determining factor when it comes to diffusion through Sigma mucin, and that the effect on the diffusions caused by G-blocks is relatively small, most probably due to the matrix of Sigma mucin, lacking the large networking polymers on which G-blocks previously have shown their effect. It was found that G-blocks make the distribution of trajectories more homogenous, but that this did not affect the mean displacements.

Sammendrag

Menneskets indre overflater er dekket med et slimlag som er en viktig beskyttelsesbarriere mot fremmede komponenter, men den skaper også restriksjoner når det kommer til levering av legemidler. Om man finner metoder for å overkomme denne barrieren vil man være mye nærmere en effektiv levering av større medisinsk aktive komponenter og nanopartikler. Nyere forskning har vist at alginat G-blokk polymerer kan modifisere de fysiske egenskapene til slim, slik at nettverket i slimet blir mer åpent og man kan få økt partikkeltransport over slimbarrierene. Dette viser at G-blokk kan være en interessant kandidat for levering av legemidler over slimbarrieren, men videre arbeid for å forstå mekanismene bak G-blokkenes interaksjon med slim er fortsatt nødvendig.

Studier har vist at nøytralt ladde partikler diffunderer lettere gjennom slim enn ladde partikler. I denne oppgaven ble interaksjoner mellom nanopartikler med ulike overflateegenskaper og komponenter i slim fra grisemage (fremstilt av Sigma) studert ved dynamisk lys spredning, og effekten av G-blokk på disse interaksjonene ble vist. Diffusjonen til partiklene ble bestemt og sammenliknet i slim fra grisemage (Sigma) ved bruk av konfokal mikroskopi og videre sporing av partiklene ved multiple particle tracking (MPT). Alginat G-blokk ble tilført partiklene og diffusjonen av disse ble sammenliknet med diffusjonen av partikler uten G-blokk.

Resultatene viste at G-blokk kan redusere mengden slim som akkumulerer på positivt ladde nanopartikler, men ikke på negativt ladde nanopartikler. Sporingen av partikler ved MPT viste at overflateladningen på nanopartiklene er bestemmende faktor når det kommer til diffusjon gjennom Sigmaslimet, og at effekten G-blokk hadde på denne diffusjonen var liten. Dette kommer mest sannsynlig av at slimet fra Sigma inneholder svært lite av de nettverksbyggende delene i slim som G-blokk tidligere har vist seg å ha en effekt på. Det ble vist at G-blokk får distribusjonen av partikkeldiffusjon til å bli jevnere, men dette påvirket ikke den gjennomsnittlige diffusjonen.

Content

1 Introduction

1.1 Aim of the thesis – motivation

The mucosal surfaces of the body are an attractive route for drug delivery but mucus provides a significant barrier to the delivery of large drugs and nanoparticles. Alginate G-blocks have shown potential to improve nanoparticle mobility in mucus but we currently do not have a complete understanding of the mechanisms behind this process.

The aim of this thesis is to increase the understanding of how G-blocks improve particle mobility in mucus by investigating whether improvements in mobility can be correlated with a reduction in interactions with mucus matrix components.

The objectives were

1. To investigate interactions between nanoparticles with different surface structures and mucus components. This was studied through changes in nanoparticle size and surface charge after exposure to mucus components.
2. To investigate whether G-blocks inhibited interactions between nanoparticles and mucus components.
3. To study the mobility of nanoparticles with different surface structures in a mucus matrix with and without G-blocks, and determine if there was a correlation between nanoparticle mobility and interactions with mucus components.

1.2 Mucus

Mucus is an important biological barrier that covers a majority of the internal surfaces in the body that are exposed to the external environment, for example the respiratory, genitourinary and gastrointestinal tracts. This sticky material is secreted from goblet cells and surface epithelial cells, and lies on top of the epithelium, where it functions both as a mechanical and a chemical protector of these cells. (Khanvilkar *et al.*, 2001, Quraishi *et al.*, 1998, Cone, 2009, Lai *et al.*, 2009a) Mucin polymers, the primary components that form the mucus gel, are built up of mucin monomers that consist of a long flexible protein backbone densely coated with short, hydrophilic glycans with negatively charged sialic acid or sufate-groups on their ends. The mucin fibers are typically 3-10 nm in diameter and 10-40 mDa. The protein backbone, composes about 20 % of the molecular mass, and consists mainly (~ 60 %) of the amino acids serine, threonine and proline in repeating STP-domains.(Bansil and Turner, 2006, Lai *et al.*, 2009b, Allen, 1983) These parts of the protein backbone are glycosylated by oligosaccharide chains consisting of 5-15 monomers, attached to the protein string through O-glycosidic bonds to the hydroxyls of serine and threonine. The glycan coverage is dense and make up about 80 % of the mucus' dry weight. The terminal regions of the mucin monomer are non glycosylated and relatively hydrophobic and have amino acid-compositions similar to globular proteins. These terminal regions are rich in cysteine allowing polymerization through disulfide bonds, as shown in figure 1.2-1.(Cone, 2009, Bansil and Turner, 2006, Sanders *et al.*, 2009, Allen and Garner, 1980) The mucin polymers are able to interact with each other, and to other surfaces, by many alternating low-affinity, non-covalent bonds, such as hydrogen bonds, Van der Waals forces, electrostatic and hydrophobic interactions. (Bansil *et al.*, 1995) The relative contribution of each type of binding is uncertain, and as shown in the PhD thesis of Taylor (2001) the interactions are complex and non-specific in nature. Because the mucins are generally negatively charged there will be repulsive forces acting between them making them stay expanded. Mucus also contains non-mucin components such as lipids, water, DNA, cells, cellular debris, proteins, Ca^{2+} and non-mucin glycoproteins. The total of repulsive and attractive mucin-mucin interactions and mucin-non-mucin interactions make the mucus gel elastic and flexible, allowing it to stay expanded, and not aggregate, but able to form interactions with neighboring molecules. This is an important property of mucus as it creates an unstirred layer on top of cells, protecting the cells. (Cone, 2009, Allen, 1983) Because the mucus is made up of multiple fibers it creates a mesh network at the molecular scale. The physical

characteristics of this network, such as pore size, depend on the concentration and entanglements of mucins.(Cu and Saltzman, 2009) This network traps almost everything that comes into contact with it, due to the multiplicity of interactions available, as mentioned previously.(Lai *et al.*, 2009a, Bansil *et al.*, 1995, Taylor, 2001) Only small, un-charged molecules have been shown to penetrate through the mucus unhindered, and to avoid mucosal adhesion.(Lai *et al.*, 2007, Wang *et al.*, 2008, Cone, 2009) On the macroscopic level, mucus is non-Newtonian and thixotropic, meaning it displays a decrease in viscosity over time at constant shear rate. If the shear is low, mucus behaves like an elastic solid and regains its shape with time. If the shear is high, mucus behaves like a viscous liquid, but when the shear is removed the mucus will regain the shape of a dynamic gel. (Lai *et al.*, 2009b) All the non-mucin components will also contribute to the viscosity in mucus, and regulation of these various components is complex and very important for the mucus to function normally. (Lai *et al.*, 2009b, Cone, 2009)

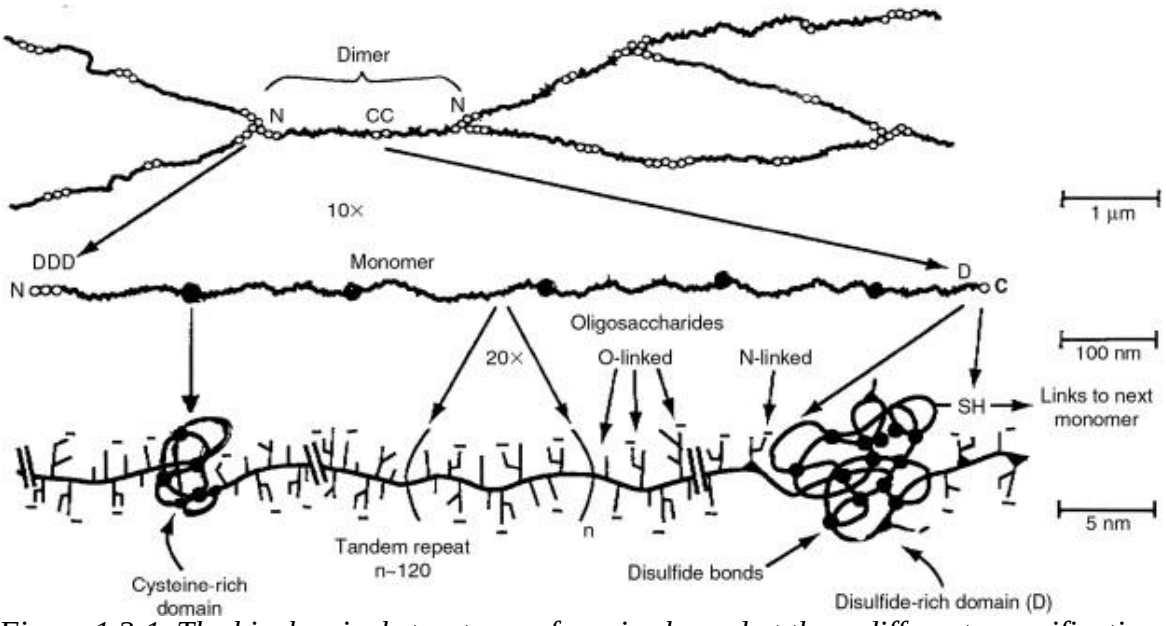

Figure 1.2-1. The biochemical structures of mucin showed at three different magnifications (Cone, 2009)

The mucus backbone in the mucin polymers are coded for by mucin (MUC) genes located on chromosome 11. 19 such MUC genes have been identified so far, giving rise to different protein backbones in addition to different glycosylation patterns. Different ensembles of these genes are expressed in different tissues, and this leads the mucus to show a large diversity in composition at different sites of the human body. (Bansil and Turner, 2006) The pH, amount of non-mucin

components, length of mucins and the thickness of the mucus layer will also vary, depending on the location in the body and the physiological state and the individual. This will affect the mucus' viscoelastic properties. (Lai *et al.*, 2009a, Taylor Nordgård and Draget, 2011, Cone, 2009, Roussel *et al.*, 1988) When doing research on mucus this is also something to consider. Native mucus contains long, and short, polymer chains and a lot of non-mucin components, figure 1.2-2A. All the different interactions occurring in this mucus matrix make it challenging to determine the relative importance of each interaction type, and each component. Purified mucus, figure 1.2-2B, is cleansed for all non-mucin components, and the majority of small parts of the polymer. This makes up a cleaner network, with more homogenous mesh spacing.(Crater and Carrier, 2010) Sigma mucin (figure 1.2-2C) contains some of the non-mucin components, relatively less high molecular weight mucin polymer and more cleaved, short polymers, leading to altered network properties compared to native and purified mucus.

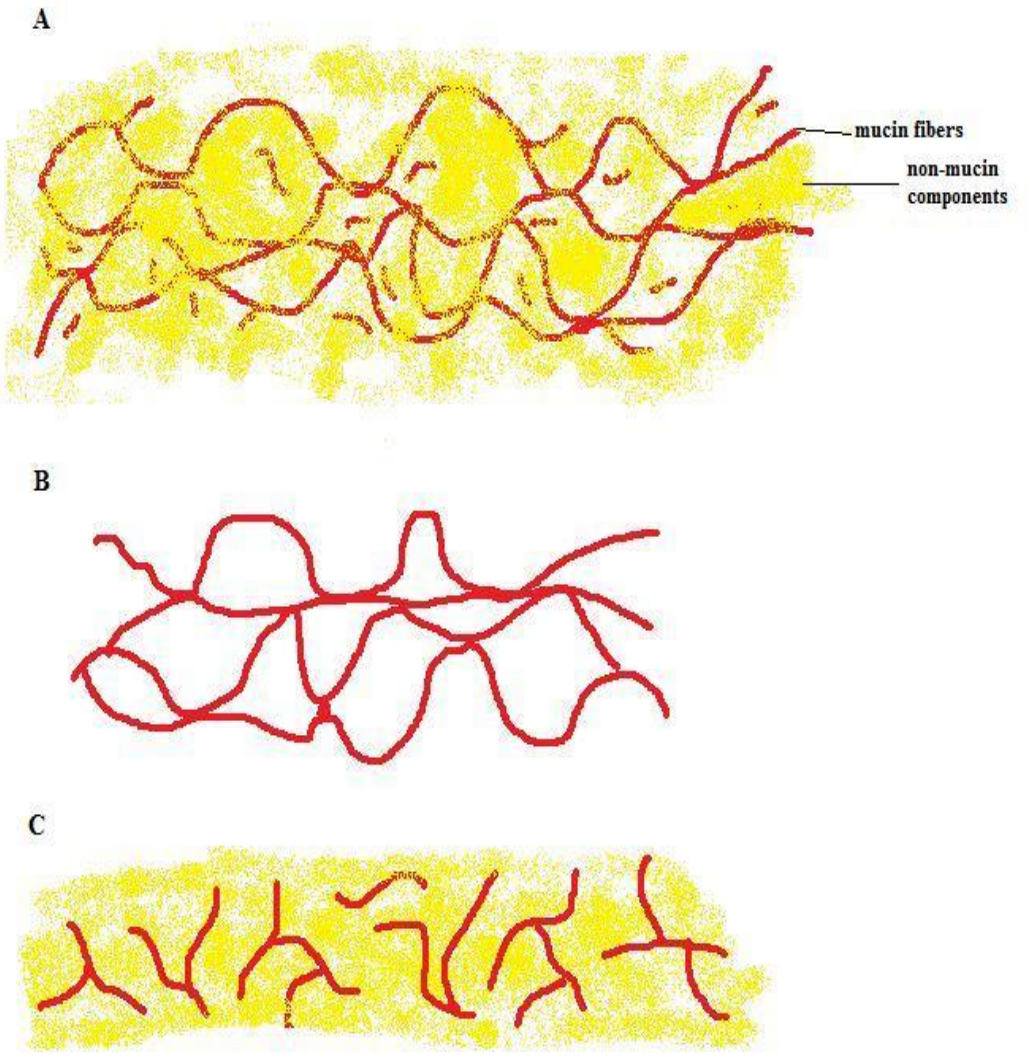

Figure 1.2-2. Imagined structures of native mucus , (A), containing long and short mucin fibers (red) and a lot of other non-mucin components (yellow), such as proteins, lipids, DNA and cell debris. B is illustrating purified mucin cleansed for everything but the long mucin fibers, creating a cleaner and more open network. C illustrates the Sigma mucin, with shorter mucin fibers and some non-mucin components. This mucus does not have the same network properties as A and B.

1.3 Barrier properties of mucus

The mucus layer covering the internal surfaces of the human body is, as previously mentioned, different from location to location, and has varying functions and functional properties at the various locations. In the stomach the mucus protects the underlying mucosal cells from mechanic abrasion, the acid gastric juices and from luminal pepsin. (Allen and Garner, 1980) In the intestine the mucus layer on top of the enterocytes protect them from being "scratched" by passing chyme, but it also inhibits macromolecular absorption from the intestine by preventing the macromolecules from reaching the cells surface. The constant secretion of mucus from the intestines creates a flow away from the cells, so molecules being absorbed must travel upstream to get to the cell surface. The mucus cover is part of the extrinsic barrier in the intestine. (Mayer and Walker, 2005) In the lungs mucus also covers and protect the epithelial cells, but it is also a central element of the mucociliary clearance system. This is an effective and absolutely necessary mechanism for the body to get rid of particles we breathe in, which settle in the mucus and are cleared from the lungs together with the mucus by the propulsion of the cilia. (Sanders *et al.*, 2009, Patton and Byron, 2007) Mucus viscoelasticity in healthy individuals can block the mobility of bacteria, leukocytes and sperm. The viscoelasticity and barrier properties of cervical mucus vary with the menstrual cycle, and the mucus is penetrable to sperm only during the time of ovulation. Nonovulatory mucus is thicker, and may prevent the entry of bacteria such as *Escherichia coli* and even sperm. (Carlstedt and Sheehan, 1989, Allen, 1983) Other mucus secretions throughout the body also function as a barrier to bacteria. Even so, some bacteria are especially well designed to penetrate and settle in normal mucus, especially *Heliobacter pylori* and *Vibrio cholerae*. (Cone, 2009, Lai *et al.*, 2009a)

Particles diffusing through mucus may possibly be hindered by two main mechanisms: an interactive barrier where particles may stick to the mucin fibers or a steric barrier where they can be trapped in "cages" or pores in the mucus, because of the size of the mesh spacing between the mucin fibers. (Olmsted *et al.*, 2001) The barrier experienced by a particle will depend on the size and surface character of that particle.

1.4 Alginates and G-blocks

Alginate is a family of polysaccharides found in brown algae (*Phaeophyceae*) and some bacteria. It is a linear co-polymer built from (1→4)-bound β-D-mannuronic acid (M) and α-L-guluronic acid (G), see figure 1.4-1a. The sequence of the copolymers are quite complex and consists of three different blocks; G-blocks (homeopolymers of α-L-guluronic acid), M-block (homeopolymer of β-D-mannuronic acid) and MG-blocks (alternating M and G) (Smidsrød and Moe, 1995, Draget and Taylor, 2011), figure 1.4-1c. It is these sequences that determine the alginates capacity to form a gel. Due to the conformation in G-blocks, as shown in figure 1.4-1b, multivalent cations may bind between the G's and bind molecular chains together to a network. This is called "the egg-box model". This explains the fact that the higher G-block content in alginate – the better its gelling capacity. (Smidsrød and Moe, 1995) This has lead to the possibility of producing alginate gels with desired properties. The alginates are at first synthesized as homopolymers of M's and enzymes are used to epimerize the alginate polymers into the desired sequence of G's and M's. A possible way is to use mannuronan C-5 epimerases produced by the bacteria *Azotobacter vinelandii.* The enzyme AlgE4 produce polyaltering sequences (MGMGMG) and AlgE6 forms long G-blocks.(Christensen, 2010, Ertesvåg *et al.*, 2009, Ertesvag *et al.*, 1995, Draget and Taylor, 2011)

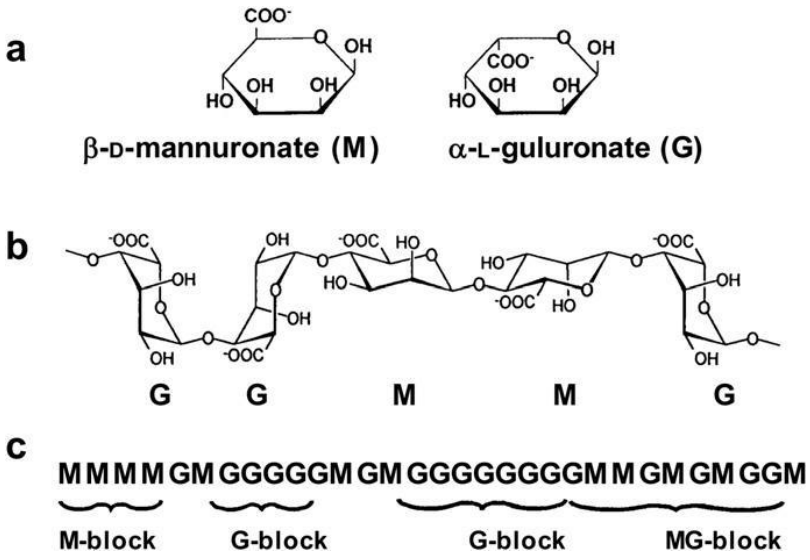

Figure 1.4-1. The structure of alginate: a) Alginate monomers, b) Chain conformation, c) Block distribution. The block distribution will vary greatly in natural alginate (Draget and Taylor, 2011, Lai et al., 2009a)

1.5 Breaking the mucus barrier

Particles diffusing through mucus can, as mentioned previously, be hindered by an interactive barrier or a steric barrier. (Olmsted *et al.*, 2001) Researchers has shown that capsid viruses diffuse freely through mucus because they have a net neutral charge, and no exposed hydrophobic regions which might make polyvalent bonds to the mucins, so they don't stick to the mucus. (Cone, 2009) This property is now being exploited as many groups make virus-mimetic nanoparticles that copy these properties and therefore diffuse relatively freely through mucus.(Olmsted *et al.*, 2001) Particles are also being covered with poly ethylene glycol (PEG) to make their surfaces neutral, and increase their diffusion through mucus (Wang *et al.*, 2008, Lai *et al.*, 2011, Lai *et al.*, 2007) and also to increase their transport rates through cytoplasm. (Suh *et al.*, 2007) PEG has been approved by the FDA (Food and Drug Administration) and is being used to improve the *in vivo* performance and stability of various non-viral drug and gene vectors.(Suh *et al.*, 2007, Sanders *et al.*, 2002, Ogris *et al.*, 2003, Lenter *et al.*, 2004, Mishra *et al.*, 2004, Zahr *et al.*, 2005, Pun *et al.*, 2004, Sun *et al.*, 2005) The PEG associates with water molecules and creates a shield surrounding the particle, giving protection against enzymatic degradation, reducing renal clearance and interactions with cell surface proteins, thereby also limiting the immunological response. These are all features beneficial for increased clinical effects. (Harris *et al.*, 2001, Harris and Chess, 2003)

In diseased states the properties of the mucus may change. There are many medications that are meant to change the properties of the mucus. These medications are collectively named mucoactive medications or mucolytic agents. (King and Rubin, 2002) The classical mucolytic agents work by disrupting disulfide bonds and thereby depolymerizing the mucins or binding calcium. The newer mucolytic agents can degrade DNA and actin. (King and Rubin, 2002, Lai *et al.*, 2009a, Lai *et al.*, 2009b)

1.6 Using G-blocks to improve particle mobility in mucus

In cystic fibrosis (CF) patients infection with the alginate producing bacteria *Pseudomonas aeruginosa* is common, and the alginate produced by this bacterium will interact with mucus in the airways creating an even firmer mucus gel. We know mucin molecules can interact and cross-link to alginates or other mucins via electrostatic interactions. (Taylor *et al.*, 2005, Taylor, 2001) These interactions can be disrupted by inserting low-molecular weight oligomers, which compete with the high-molecular weight alginate for the binding sites on mucin. G-blocks are chosen as this low-molecular weight oligomer because previous studies has shown that alginates can have immunologic properties (Draget and Taylor, 2011), but not in the case of guluronate oligomers.(Otterlei *et al.*, 1991) Experiments conducted by Taylor Nordgård and Draget, have revealed that low-molecular-weight G-blocks disrupt the intermolecular interactions in mucous systems, changing the rheology to a less cross-linked system, and decreasing the deformation resistance, figure 1.6-1. (Taylor Nordgård and Draget, 2011, Draget, 2011)

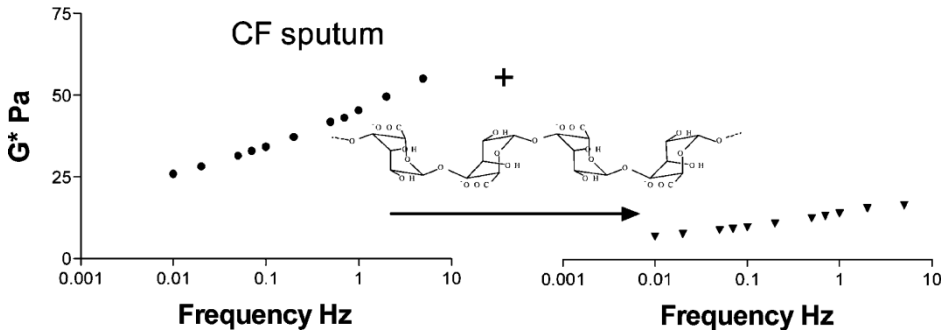

Figure 1.6-1. The figure shows the effect of G-blocks in cystic fibrosis (CF) sputum. The graph to the right visualizes how CF sputum shows a reduced resistance to deformation after G-block treatment. From (Taylor Nordgård and Draget, 2011)

It is natural to think that a decrease in resistance to deformation also implies a reduction in barrier properties. Both of these properties are related to structure of the matrix and intermolecular interactions, but altering one does not necessarily alter the other. (Dawson *et al.*, 2003, Lai *et al.*, 2009c) Recent studies by Taylor Nordgård actually show that G-blocks also improve particle mobility through mucus. By studying particle mobility by FRAP (Fluorescence Recovery After Photo-bleaching) she shows that both 200 nm and 100 nm particles show an increase in mobility by the addition of G-blocks. She also shows how this effect is seen in native pig gastric mucin

and purified pig gastric mucin. As these results show, given in figure 1.6-2, the recovery after photo bleaching is highest for particles in native pig gastric mucus (1.6-2B). Taylor Nordgård explains the greater improvement in native mucus compared to purified mucus, in unpublished work, by the fact that the purification process removes non-mucin components from the mucus network, giving the possibility of an increased number of possible binding sites for particles on the mucins.

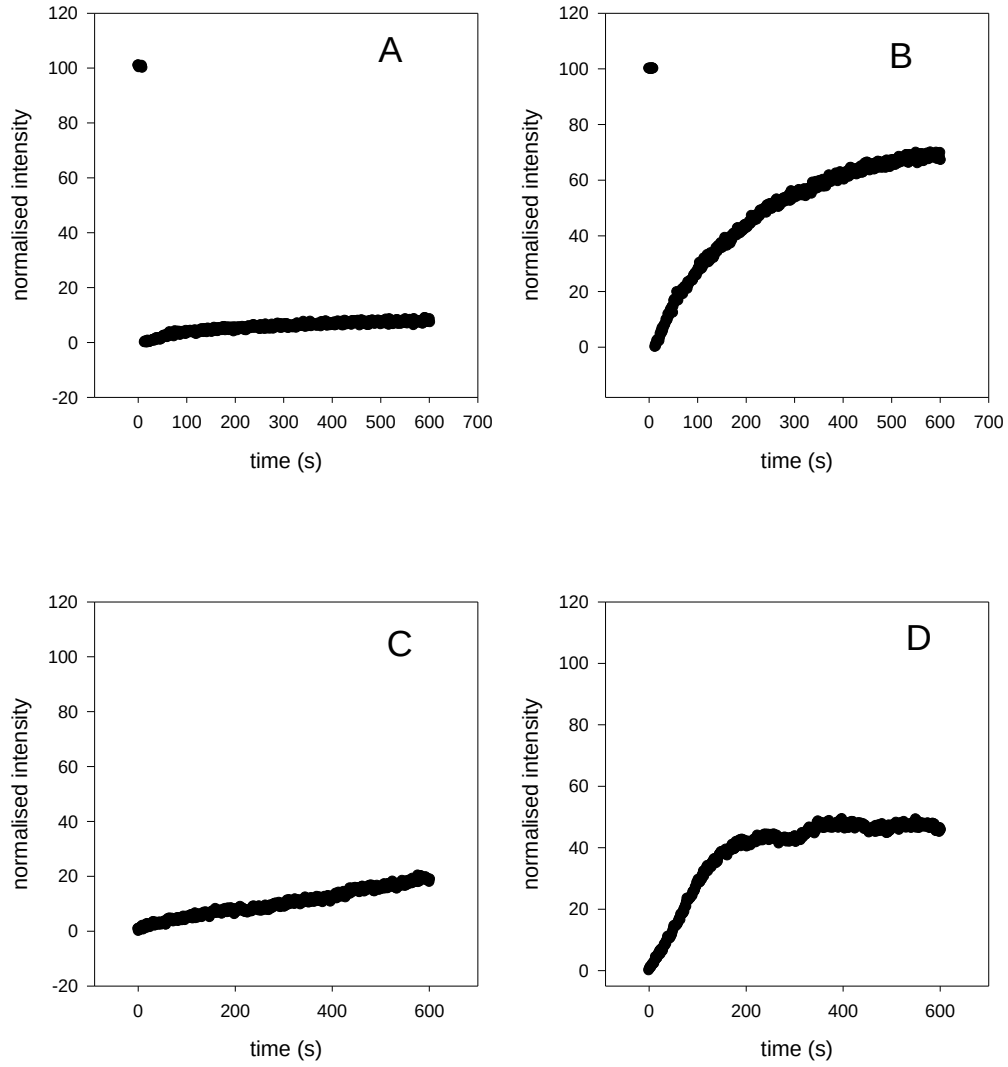

Figure 1.6-2. The figure shows FRAP intensity curves for 200 nm carboxyl fluospheres in native pig gastric mucus (A and B) and 20 mg/mL purified pig gastric mucus (C and D), with (B and D) and without (A and C) 4.8 mg/mL G-blocks. The curves show how the intensity in the bleached areas are regained in the samples containing G-block, and how it remains low in the samples without G-block. Experiment by C.Taylor Nordgård, unpublished work.

The same group has also showed that G-blocks alter the network structure in native pig gastric mucus. Figure 1.6-3 shows SEM pictures of a native pig gastric mucus matrix without and with added G-blocks. These pictures show how the spacing between mucin fibers becomes larger by adding G-blocks.

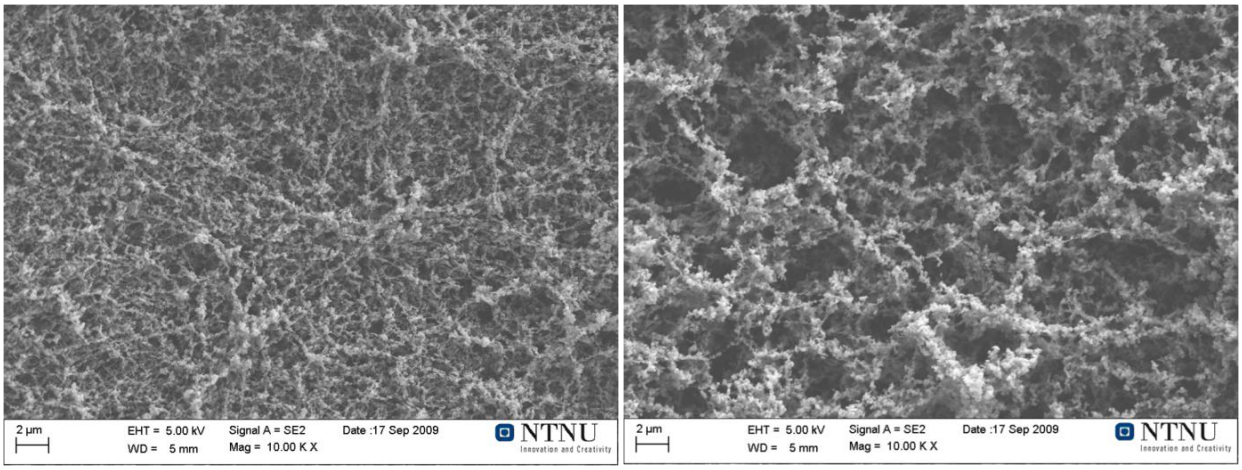

Figure 1.6-3. The figure shows SEM pictures of pig gastric mucus network structure with (right) and without (left) G-blocks. The picture to the left, without G-blocks, shows a more cross-linked system. After addition of G-block, right, the system is more open and one may actually see increased pores in the network. These findings lead to further curiosity concerning G-blocks as a mucus modulator, and their use in drug delivery. (Pictures are captured on a S-5500 SEM microscope at the NTNU nanolab, in courtesy of professor Kurt I. Draget and Magnus Olderøy, PhD 2009)

The alternations caused by G-blocks in the presented studies promote G-blocks as an interesting proposition in future drug delivery across mucosal barriers. It has been shown that they alter the rheology, improve mobility through mucus and alter the network structure. A question that remains is whether or not G-blocks also are able to alter the interaction barrier between particles and mucus. Understanding the mechanism of action of G-blocks will help in determining the applications of G-blocks in drug delivery.

1.7 Theory

To determine whether G-blocks are capable of changing the interaction barrier between nanoparticles and mucus components, the nanoparticles were studied in a Zeta Sizer to investigate changes in size and surface potential. Then multiple particle tracking (MPT) was conducted and the data from the two methods was analyzed for correlation.

1.7.1 Zeta Sizer

A Zeta Sizer uses dynamic light scattering (DLS) to measure particle size in solution. The sample is illuminated by a laser, and the particles in solution will spread the light. This light is captured by the device and a speckle pattern is detected. Due to Brownian motions particles in a liquid are never stationary, and the speckle pattern will change with time. The instrument compares the speckle pattern at different time points and creates a correlation function. The size, as hydrodynamic radius, is interpreted through the correlation function and the Stokes-Einstein relationship (equation 1) to give an intensity distribution (Hiemenz and Rajagopalan, 1997, Malvern, 2004). This intensity distribution can be converted to a volume distribution which can then be converted to a number distribution. (Malvern, 2004, Doak *et al.*, 2010)

$$D = \frac{k_B T}{6\pi\eta \mathrm{R}} \qquad (1)$$

k_B is the Boltzmann constant, T is temperature, η is the viscosity of the fluid and R is the hydrodynamic radius of the particles. From the intensity distribution the polydispersity (PDI) is also found. If PDI > 0.5 the method is not adjusted to fit the real data, and the measurements should not be used.

Charged particles will make ions from the surrounding environment adjust to these charges. Ions of opposite charge will be attracted to the particle surface and this creates an electrical double layer around each particle (figure 1.7.1-1). This layer and the liquid it holds can be divided into two layers: the inner, Stern, layer where the ions are strongly bound and the outer, diffuse, layer where the ions aren't that strongly bound. The ζ-potential is the potential existing at the surface of hydrodynamic shear, or the slipping plane, surrounding the particles. (Hiemenz and Rajagopalan, 1997)

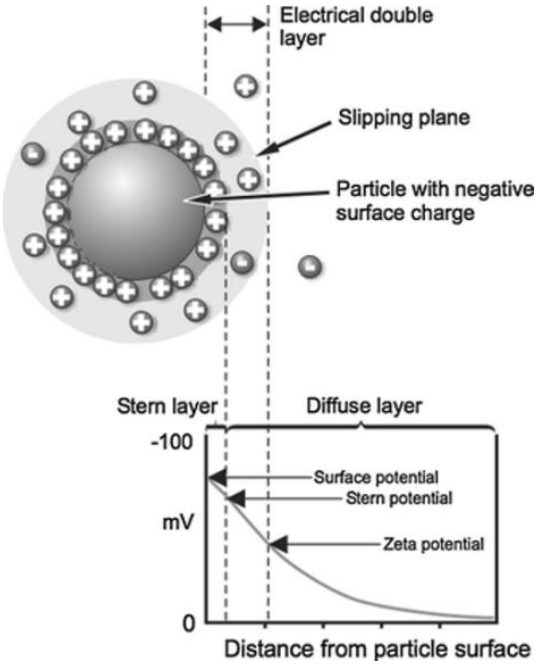

Figure 1.7.1-1. Overview of the liquid layers surrounding a negatively charged particle. The ζ-potential is the potential measured at the slipping plane. From (Malvern, 2004)

The Zeta Sizer calculates the ζ-potential by electrophoretic mobility. A cell with electrodes at each end is used, and particles will move towards the electrode of opposite charge. The velocity of the moving particles is measured using a combination of Laser Dopler Velocimetry (LDV) and M3 Phase Analysis Light Scattering (M3-PALS), and then applying the Henry equation to give the ζ-potential. (Malvern, 2004) Since these measurements rely on electrophoresis, the viscous forces in the suspension will make an impact. If components in the suspension tend to aggregate onto the particles while measuring, these components will subsequently be removed from the suspension possibly causing the viscosity in the suspension to change. This will create inaccuracies in the measurements.

SOPs can be set up if parameters are to be kept consistent for repeated measurements. By using SOPs the addition of parameters is only set once and the risk of introducing errors in the settings is minimized.

1.7.2 Multiple Particle Tracking (MPT)

Multiple particle tracking (MPT) has been developed as a high throughput method for single particle tracking (SPT). MPT uses video microscopy to track the motions of individual particles simultaneously. The video can be taken with extremely high temporal resolution, and give a position for every particle at every timeframe. The concept of timeframe may not be intuitive, so this will be further explained. When a movie is captured, for example at 30 frames/s for 20 seconds, the total number of frames is 600. The time interval between each frame becomes (seconds/total number of frames) 33 milliseconds (figure 1.7.2-1). The 600 framed movie results in 599 displacement values. The next shortest time frame is 66 milliseconds, and there will be 598 displacement values for this time frame. So, time scale is the time a particle is allowed to move before we calculate it's displacement from an initial point.(Suh *et al.*, 2005)

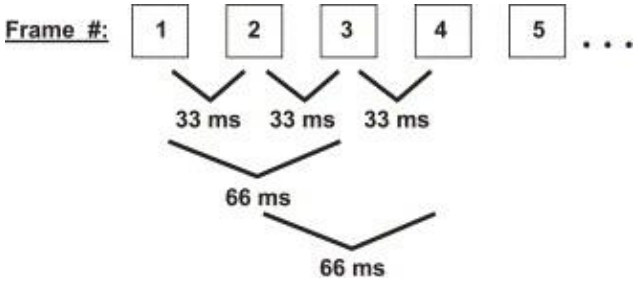

Figure 1.7.2-1. The figure illustrates the time scale for a movie captured at 30 frames/sec for 20 seconds. Time scale must be interpreted as the time a particle is allowed to move before measuring it's displacement from the initial point. From Suh (Suh et al., 2005)

To perform MPT confocal microscopes can be used. A confocal microscope uses laser light to illuminate the sample, and pinholes to exclude out-of focus light. This method allows one to capture very clear pictures of thicker samples, and to image individual planes in a thick object (optical sectioning). These microscopes use photo multiplier tubes (PMT) as image capture devise.(Cox, 2007) Movies are captured of particles moving in a solution or matrix. These movies can then be analyzed by suitable software to obtain information on individual or ensamble transport properties. As x and y positional data are found by the software, mean-square displacement (MSD) and effective diffusivities (D_{eff}) can be obtained by the following formulas.

$$MSD = [x(t+r) - x(t)]^2 + [y(t+r) - y(t)]^2 \quad (2)$$

$D_{eff} = (MSD) / 4\tau$ (3)

where τ is the time lag. (Crater and Carrier, 2010)

Log-log plots of MSD against timescale will show the type of mobility as the slope (α – the anomalous exponent). If $\alpha > 0.9$ the particles are diffusing freely, if $\alpha < 0.9$ the particles undergo subdiffusive transport, and if $\alpha < 0.2$ the particles are considered immobile. Similar log-log plots of D_{eff} against timescale would show diffusion as a flat line, subdiffusing transport as D_{eff} becoming lower with increasing τ, and active transport as a curve increasing with τ (figure 1.7.2-2). (Suh *et al.*, 2005) When a subdiffusing D_{eff} curve decrease at short time scales and moves towards a constant value at longer timescales (as for the line in figure 1.7.2-2), this indicates that you are dealing with mesoscopic diffusion. In mesoscopic diffusion the particles are on the size scale as the network pores, and seem trapped in these pores at short timescales. At longer timescales the particles appear diffusing because of their movement across these pores. (Suh *et al.*, 2005) This indicates that it is necessary to consider the size of the particles and the length scale studied before drawing conclusions about the particles transport mode. The possibility of tracking each particle, and looking at their diffusivities gives this method a benefit as when compared to Fluorescence Recovery After Photobleaching (FRAP), which gives ensemble averages, since a distinct area is bleached and the total fluorescence recovery is measured rather than the single particles contribution.

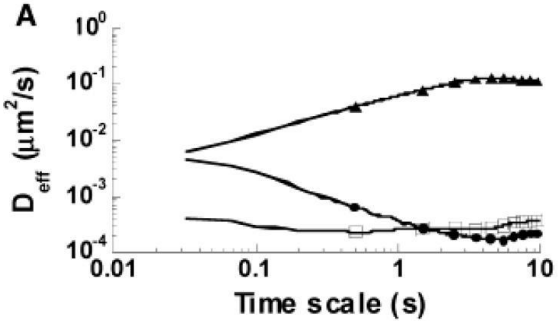

Figure 1.7.2-2. Different transportmodes of particles can be classified into three groups based on their D_{eff} curves. Diffusive (□), subdiffusive (●) and active (▲). From (Suh et al., 2004)

1.7.3 Choosing Sigma mucin

As explained earlier native mucus, purified mucus and Sigma mucin do not consist of the same components even when being extracted from the same source (in this case pig stomach). Since it was desirable to study the interactions between nanoparticles with different surface structures and mucus components by a Zeta Sizer it was important to choose a mucus which would not cause any significant affect on the viscosity in the system. As mentioned previously, high molecular weight components adsorbing on to a particle and thereby being removed from the solution may cause a change in viscosity, interfering with the electrophoretic mobility measurements and causing misleading results. This would be likely to happen if the chosen mucus contained a lot of large polymers. If these polymers then adsorbed on to the particles they would cause the particles to grow and the viscosity in the system to decrease, and these two effects may cancel each other out in measuring electrophoretic mobility. To avoid this happening, and allow us to still investigate the surface interactions on the particles, Sigma mucin was chosen for this work since this mucus type contains primarily shorter mucin polymers not altering solution viscosity to the same degree.

2 Materials and methods

2.1 Materials

2.1.1 Particles (FluoSpheres)

Carboxylate-modified FluoSpheres and Amine-modified FluoSpheres were purchased from Invitrogen. These are made by the producer by grafting polymers with carboxylic groups to sulfate microspheres 0.2 µm in diameter. These microspheres are highly charged and relativly hydrophilic, but because the particles are polystyrene-based, they will always retain some hydrofobicity. The amino-modified microspheres are created by the distributer by further modifying the carboxyl-microspheres. The fluosphere particles are kept as suspensions with 2 % solids in water, with 2 mM sodium azide. (Invitrogen and MolecularProbes, 2005, Invitrogen and MolecularProbes, 2004) The size and Zeta-potential of the particles was determined by dynamic light scattering in a Zeta Sizer Nano from Malvern at a particle concentration of 0.0025 wt %, se section 2.2.1. The particles used were red (ex. 580 nm and em. 605 nm), and yellow-green (ex. 505 nm and em. 515 nm). (Invitrogen and MolecularProbes, 2005).

2.1.2 Porcine mucus

The mucus used in this assignment was originally extracted from pig stomach, and was of the type II Crude from SIGMA (M-2378, Lot. 26H1004). This was diluted in water to 1000 µg/mL and filtered firstly with a 1 µm syringe filter and secondly with a 0.2 µm syringe filter. This was done to remove aggregates > 2000 nm. Both unfiltered and filtered mucin was observed in the Zeta Sizer. Sigma mucin was diluted to three different concentrations each with 10 mM NaCl for the time study (750 µg/mL, 500 µg/mL and 100 µg/mL).

For the MPT the same Sigma mucin was diluted in 0.05 M NaCl to different concentrations (30 mg/mL, 45 mg/mL, 60 mg/mL and 120 mg/mL) but not filtered as all components were wanted in the studied mucus matrix.

All mucus samples were kept in closed containers for a maximum of one week, at a stir plate at 4°C, to minimize bacterial growth.

2.1.3 G-block F-41-07

The G-block fraction used in these experiments was produced in 2007 by the group of Prof. Draget. It was obtained by acid hydrolysis of high molecular weight alginates with a high content of guluronic acid residues as previously reported.(Haug *et al.*, 1966, Haug *et al.*, 1967) Chemical composition and sequence, determined by 1H-NMR spectroscopy (Grasdalen, 1983) showed the fractions of guluronate containing monad (F_G), diad (F_{GG}) and triad (F_{GGG}) were 0.94, 0.83 and 0.80, respectively. The distribution and number-average degree of polymerization (DP_n) of the G-block sample used has been quantified as described earlier (Gimmestad *et al.*, 2009) using a HPAEC-PAD (Dionex BioLC System, Dionex Corporation, Sunnyvale , Ca). This showed an average DP_n = 12 with 40 % of the molecular population in both the DP range of less than 10 as well as in the range 10-20. No high molecular weight tail was observed.

2.2 Methods

2.2.1 Dynamic Light Scattering (DLS)

A Zeta Sizer Nano ZS90 from Malvern Instruments was used to perform dynamic light scattering (DLS). This device uses a HeNe laser (632.8 nm) to determine particle size, molecular weight and zeta-potential (ζ-potential) from scattered light detected by 90° detection optics (Malvern, 2011). SOPs were used for all measurements and all settings can be found in appendix A. The light scattering was performed on 0.0025 wt % particles in 10 mM NaCl. This was prepared by mixing A: 350 µL water and5 µL of the original 2 % particle solution B: 350 µL water and 30 µL of dilution A. Then 17 µL 0.2 M NaCl was added to B. When studied with Sigma mucin the 17 µL NaCl was exchanged with 17 µL of the different mucus concentrations (10 mM).

2.2.2 PEG-ylation of particles

5000 Da α-Methoxy-ω-amine polyethylene glycol (figure 2.2.2-1) was purchased from chemicell (PMA5-5, 1210/11). Carboxyl particles was PEGylated according to a PEGylation protocol prepared from Molecular Probes Invitrogen (Invitrogen and MolecularProbes, 2004) combined with the methods described by Suh (2007), se appendix B. At step 9 and 11 the centrifugation had to be done over longer time intervals, as a centrifuge with high enough speed was not available. The maximum speed available was 11 000 rpm. The pellet did not get as compact as presumed, and some particles was probably lost with the supernatant. At the end the pellet was dissolved in 5 mL water, to obtain the same concentration of particles as the original purchased particles, 2 wt %.

The PEG covered particles was then observed in the Zeta Sizer to determine the size and ζ-potential. Size measurements by this apparatus showed to high PDI-values so the particles were observed in an inverted light microscope from Nikon (Eclipse TS100). Aggregation was observed and multiple rounds of sonication in a water bath sonicator were conducted to separate aggregates. After sonication the size and zeta-potential of the particles could be determined with the Zeta Sizer.

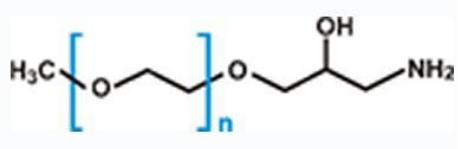

Figure 2.2.2-1. α-Methoxy-ω-amine polyethylene glycol was purchased from chemicell and used to make neutral particles from carboxyl particles. (chemicell, 2011)

2.2.3 Multiple particle tracking

In this assignment, a Leica confocal TCS SP5 microscope type DMI6000 was utilized. The diffusion experiments were performed on chambered, non-fluorescent borocilicate coverglass systems from Lab-Tek, with a 63x magnification water immersion lens with numerical aperture 1.20 at room temperature. 10 µL of diluted particle solution (0.0025 wt %) was added and stirred into 0.2 g of mucus. 20 s videos were captured from different preparations for a total of ± 100

particle trajectories for each particle type, for each preparation. With active resonance scanning the captured 20 s movies obtained consisted of 279 frames, resulting in the shortest time frame being 0.07 s.

The mucus itself showed some fluorescence so the settings were adjusted to remove this. The chosen settings are shown in appendix C. Examples of captured movies can be found as .avi-files in the enclosed CD. All original movies can be found as .lif-files on a portable hard drive at the office of Prof. Draget.

2.2.4 Data analysis

The data from the MPT was analyzed by ImageJ and Matlab. To import the files from the Leica confocal to the ImageJ image analysis software, an ImageJ plugin; *LOCI bio-formats*, was installed, and to analyze the trajectories to obtain XY coordinates over time another plugin, the *SpecleTrackerJ* was installed. All plugins are free from the ImageJ web-page.

From SpeckleTrackerJ all particle XY-positions were exported as a .txt-file that could be analyzed by Matlab. A Matlab-code was created to convert all XY-values into mean square displacement (MSD) values, se code in appendix D. These MSD-values were then further analyzed in SigmaPlot and Exel to get the effective diffusion constants (D_{eff}) and their square values. Log-log plots of MSD and D_{eff} against timescale were created. A detailed description of the data analysis is available in appendix E.

3 Results and discussion

3.1 Particle size and the effect of mucus and G-blocks

The original size of the particles received from Invitrogen was 200 nm. This size is measured by electron microscopy.(Invitrogen and MolecularProbes, 2005) The Zeta Sizer measures size by hydrodynamic radius, which include all associated water molecules, so these size measurements is expected to be larger. The diameter size of the purchased particles was in the Zeta Sizer measured to be 244 ± 1.5 nm for the carboxyl particles and 240 ± 1.4 nm for the amine particles.

3.1.1 Determining a suitable Sigma mucin concentration

Three different Sigma mucin concentrations were investigated together with the particles to find a concentration suited for the further experiments. The concentrations were 750 µg/mL, 500 µg/mL and 100 µg/mL Sigma mucin diluted to 10 mM NaCl. The size of the different particles in these mucin concentrations was investigated each hour, for three hours. Measurements showed that unfiltered mucus created aggregates > 1000 nm, and filtered mucus showed aggregates about 100 nm in size. For the filtered mucus with particles the observed diameters are given in table 3.1.1-1.

Generally the carboxyl particles show less mucin aggregation, and size increase, than the amine particles. This may be explained by the charges. The mucin is more negatively charged than positive, so there will be more attraction between the mucus and the positively charged amine particles, than between mucin and the negatively charged carboxyl particles which may even show repulsion due to the net negative charges. As such this result was as expected. The increase in size is generally greater with higher mucin concentrations, something that would also be expected considering the mucus' networking properties. That the amine particles show more aggregation and larger sizes in both 750 µg/mL and 100 µg/mL, than in 500 µg/mL is peculiar. It is possible that this variation reflects errors in the sample or inaccuracies in the system.

The particles show no clear tendency of increasing in size with time. This is only seen for the particles in the highest mucin concentration (750 µg/mL), and for the amine particles in the lowest concentration. This may indicate increasing mucin aggregation on particle surface. In the

other mucus concentrations it seems the particles reach a dynamic equilibrium with the mucus, and that the amount of mucus adding to the particles is relatively equal to the amounts detaching over time.

Table 3.1.1-1. The size of particles in three different mucus concentrations was investigated each hour for three hours. The results showed that the mucus concentration of 100 µg/mL showed the least aggregation to the particles. The sizes represent the diameter of the particles in nanometers (nm).

	750 µg/mL Sigma mucin			**500 µg/mL Sigma mucin**			**100 µg/mL Sigma mucin**		
	1 hr	2 hr	3 hr	1 hr	2 hr	3 hr	1 hr	2 hr	3 hr
COOH-particles (d.nm)	317 ± 8.7	318 ± 2.1	322 ± 4.9	305 ± 4.7	303 ± 1.0	303 ± 1.7	276 ± 1.2	269 ± 5.8	273 ± 3.0
NH_2-particles (d.nm)	536 ± 7.4	590 ± 8.6	590 ± 23.3	302 ± 5.7	293 ± 4.9	296 ± 2.6	340 ± 5.1	378 ± 9.0	404 ± 3.1

In addition to the sizes interpreted to be particles, listed in table 3.1.1-1, bigger peaks were observed for the amine particles in the highest and in the lowest mucus concentration. These peaks were > 4000 nm and therefore probably Sigma mucin aggregates. The amount of these aggregates increases over time. In the highest mucus concentration they go from making up 3.9 % of the total volume to making up 8 % of the total volume. In the lowest mucus concentration this increase is from 2.7 % to 10.9 %. This indicates that mucus aggregation occurs over time.

From these experiments the Sigma mucin concentration of 100 µg/mL was chosen as the best one for further work as particles in this concentration showed least aggregation. Further work was to

be done on carboxyl particles, amine particles and PEG covered particles, so PEGylation was conducted next.

3.1.2 PEGylated particles

Straight after PEGylation the particles showed aggregation, something solved by vigorous sonication. Figure 3.1.2-1 shows the pictures of the original particles (A), the PEGylated particles straight after PEGylation (B), and the PEGylated particles after sonication (C). After the agglomerates had been dissolved, the size was measured in the Zeta Sizer. The size of the particles was increased by the addition of PEG. The size obtained was about 700 nm larger in diameter than the original carboxyl particles. This increase was not expected. Other has shown that the same PEGylation process has lead to a size increase of only 15.7 nm and 21 nm by Lai (2007) and Wang (2008) respectively. It must be considered a possibility that some agregates still remain, as also the picture in figure 3.1.2-1C does not show exactly the same as A. This also correlates with the Zeta Sizer data which showed some peaks for particles with diameters > 5000 nm. These peaks most probably represent aggregates of PEGylated particles.

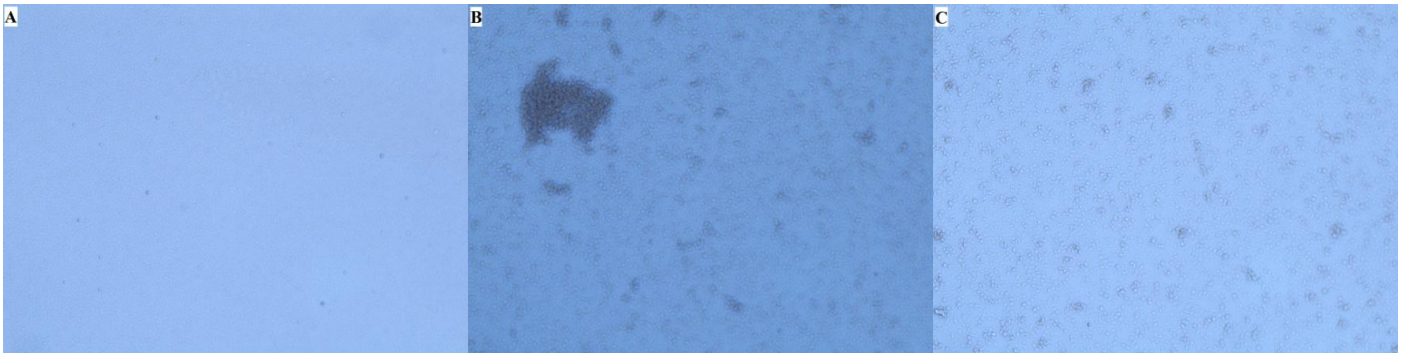

Figure 3.1.2-1. The PEG coated particles showed aggregation straight after PEGylation. The original carboxyl particles (A) showed a much more homogenous size distribution than the PEG covered particles (B). After sonication the particles became less aggregated (C). Photos captured by a Nikon Eclipse TS100.

3.1.3 The effect of Sigma mucin and G-blocks on particle size

After PEGylation the three different particles were studied over time in Sigma mucin and in G-block *and* Sigma mucin. The results are given in table 3.1.3-1 and 3.1.3-2. All measurements were done in series of three, and the given values are the average of these three. The measurements of particles in mucus, both with and without G-block, were conducted as a time-dependent measurement. In these the series of three was repeated with one hour interval for two hours.

Table 3.1.3-1. Size measurements of particles in Sigma mucin (100 µg/mL) done over a timescale of two hours. The given sizes are averages of three measurements done in sequence at each measure round.

Particle type	Size (d.nm) measurement 1	Size (d.nm) measurement 2, after 1 hr	Size (d.nm) measurement 3, after 2 hrs
COOH	276 ± 1.2	269 ± 5.8	273 ± 3.0
NH_2	340 ± 5.1	378 ± 9.0	404 ± 3.1
PEG	973 ± 28.8	1034 ± 52.8	966 ± 99.5

This shows that all three particle types show stable sizes over time, with the largest increase in size seen for the amine particles. This was also observed in the first study with different Sigma mucin concentrations. The PEGylated particles are larger than the others, but the size change with time is not noteworthy.

Particles in G-block and mucus were also studied over time. The results are given in table 3.1.3-2. The values given are the averaged values for three measurements done in sequence every hour.

Table 3.1.3-2. Size measurements of particles in G-block (0.05 µg/mL) and Sigma mucin (100 µg/mL) done over a timescale of two hours. The given sizes are averages of three measurements done in sequence at each measure round.

Particle type	Size (d.nm) measurement 1	Size (d.nm) measurement 2, after 1 hr	Size (d.nm) measurement 3, after 2 hrs
COOH	310 ± 4.9	313 ± 7.2	318 ± 4.0
NH_2	296 ± 4.9	293 ± 2.4	287 ± 2.1
PEG	711 ± 15.9	640 ± 53.2	704 ± 22.2

From table 3.1.3-2 it may be said that the change induced over time on G-block covered particles in mucus is minimal. Comparing table 3.1.3-1 and 3.1.3-2 leads to the point that the G-blocks have an effect of the particle size, making the hydrodynamic radius of amine and PEGylated particles in Sigma mucin smaller than without G-blocks. The study showed that the amount of aggregation did not increase over time. This shows that once the particles are sufficiently covered with mucus, the aggregation process stops, and time is not critical for the size.

As a summary the collected results are given in table 3.1.3-3. The results given in table 3.1.3-3 for the measurements of particles in Sigma mucin and in G-block and Sigma mucin, are the average of the series of measurements done at time 1, immediately after addition of mucus described above.

Table 3.1.3-3. Size measurements done with Zeta Sizer Nano on all three particle-types; pure particles, in Sigma mucin, in G-block and in G-block and Sigma mucin.

Particle type	Pure particles (d.nm)	Particles in Sigma mucin (100 µg/mL) (d.nm)	Particles in G-block (1.1 mg/mL) (d.nm)	Particles with G-block in Sigma mucin (d.nm)
COOH	244 ± 1.5	276 ± 1.2	272 ± 7.4	310 ± 4.0
NH_2	240 ± 1.4	340 ± 5.1	295 ± 6.3	296 ± 4.9
PEGylated	953 ± 20.3	973 ± 28.8	970 ± 15.3	711 ± 15.9

For the carboxyl particles, the addition of mucus and the addition of G-blocks had a very similar effect on the size. Both of these components increased the particle size diameter by about 30 nm. This is probably explained by the charges on the molecules. The negative particles will not attract the negative mucins, or G-blocks. The particles exposed to both Sigma mucin and G-block show that the size of the particles increases. This is counterintuitive considering the particles and the G-blocks are negatively charged and the mucin has a net negative charge. There is a chance that this increase in size can be explained by cationic non-mucin components, causing an addition of mucins to the particles and that this process is somewhat enabled by G-block, since the effect is not seen in Sigma mucin alone.

For the amine particles the size increase induced by Sigma mucin was larger than the one induced by G-blocks, and they were both larger than the increases seen on the carboxyl particles. This will be explained by the charges of the molecules. The positive amine particles will attract the negative mucins, and G-blocks. That the mucus shows a larger aggregation may be due to Sigma mucin self aggregating on the particles, and the mucins are also larger than G-blocks. G-blocks will not self aggregate due to their higher charge density. This could also be the reason why the

size of amine particles with G-block in mucus is similar as when in G-block. It seems the mucus doesn't affect them much, maybe due to the high density of negative charges on the G-blocks causing repulsion of the net negative mucus.

That both mucus and G-block showed less aggregation on the PEGylated particles, than on any of the others, may be due to the fact that the PEG acts as a steric barrier against absorption of Sigma mucin and its components, as explained for intracellular components by Suh (2007).

These values suggests that there is more Sigma mucin aggregation on amine particles than on carboxyl particles as stated before, but they also indicate that G-blocks can reduce Sigma mucin aggregation on positive particle surfaces, but not on negative surfaces. If G-blocks can reduce mucin aggregation on positive particle surfaces, it is reasonable to assume that G-blocks may reduce interactions between positive particles and network components in a mucus gel. This should then, hypothetically, lead to better mobility through the mucus matrix for these particles. Also PEGylated particles show a smaller hydrodynamic radius in presence of mucus and G-blocks than with neither of these components. This implies that the PEG chains are packed more tightly around the particles when G-blocks and Sigma mucin are added. Compared to the original particles the PEGylated particle surface is covered with a "forest" of PEGs. This "forest" might be considered soft, and a tighter packing of it would allow for the particles hydrodynamic radius to become smaller.

3.2 Particle charge and the effect of mucus and G-blocks

The ζ-potentials for the different surfaces were measured at pH values ranging between 5 and 7 using a Zeta Sizer Nano (Malvern Instruments Ltd.). Measurements were done for particles alone, particles in G-blocks, in Sigma mucin and in both. The averages of three measurements and their standard deviations are given in table 3.2-1.

Table 3.2-1. The table shows the measured values of the ζ-potential for particles alone, particles in G-block, Sigma mucin and in both G-block and Sigma mucin. The values given in the table are averages with standard deviations of three measurements, done in sequence at pH ranging between 5 and 7.

Particle type	ζ –potential of particles alone (mV)	ζ –potential of particles in Sigma mucin (100 µg/mL) (mV)	ζ –potential of particles in G-block (1.1 mg/mL) (mV)	ζ –potential of particles with G-block in Sigma mucin (mV)
COOH	-43 ± 1.18	-31 ± 1.2	-61 ± 1.0	-13 ± 0.1
NH_2	8.5 ± 1.6	-6 ± 0.5	-57 ± 1.0	0.01 ± 0.1
PEGylated	-29 ± 0.25	-20 ± 3.4	-47 ± 1.5	-32 ± 3.1

The ζ-potentials of the particles alone was as shown in table 3.2-1 negative for the carboxyl particles and positive for the amine particles, just as expected. The PEGylated particles also had a negative ζ-potential of -29 ±0.25 mV. This reveals that the degree of PEG coverage was incomplete, the ζ-potential only being increased by ~24 mV, from -43 ± 1.18 mV for the carboxyl particles to -29 ± 0.25 mV for the PEG covered particles. This was not as good a coverage as reported by Wang (2008) and Lai (2007) who reported the ζ-potential of their particles as -2 ± 4

mV and -2.1 ±0.3 mV respectively. The PEG derivates that were used here was quite large, 5 kDa. Others have tested PEG with this molecular weight and concluded that a critical molecular weight for the PEG exists between 5 and 10 kDa, within somewhere there is a transition from mucoinert to mucoadhesive. They also show that even for small PEG (2 kDa) there must be a high degree of surface coverage for the particles to retain the diffusive properties. (Wang *et al.*, 2008) This indicates that the PEG used here are in the upper size range of what have been proven effective, and that the degree of surface coverage is most probably too low to obtain the mucoinert properties.

In Sigma mucin the ζ-potential of the carboxyl and PEG particles became more positive, but the amine particles became more negative. This suggests interactions between negative particles and a fraction of Sigma mucins with positive charges, resulting in a more positive charge. The amine particles become more negatively charged, probably due to the addition of mucus to them, something also represented through the size measurements, where this particle type showed the largest size increase.

The ζ-potential of all the particles in G-block is lower than for the particles in mucus. This is not so surprising considering Sigma mucins has a lower charge density than the G-blocks, and also contain positive charges. That the charge on the particles in G-block is lower than the charge on the pure particles is due to the charge density on G-blocks adding further negative charges to the particles. The amine particles in G-block are smaller and more negatively charged than in Sigma mucin. This confirms that G-blocks add more negative charges to the particles without adding a great volume as mucus. This is to be expected because G-blocks will not self aggregate.

For G-block covered particles in Sigma mucin the ζ-potential is raised from when with only G-block or only in Sigma mucin. This suggests that there are components in the Sigma mucin pulling the charge up on the particles. This is especially noticeable for the carboxyl particles, as these particles become less negatively charged, and larger. This indicates interactions with regions of mucus which are positively charged, and possibly self aggregation of mucin. Since the particles in G-block and Sigma mucin got larger than those in only Sigma mucin, the G-blocks must be a factor for this size increase.

Both size and ζ-potential measurements of amine particles in Sigma mucin, G-block and Sigma mucin and G-block support the theory that G-blocks may reduce interactions between positive particles and Sigma mucin. For carboxyl particles the results suggests that there are interactions between the particles and positively charged regions of mucus, and these are apparently increased when G-blocks are added. For PEGylated particles there are no clear indications of how interactions are effected, even though a great decrease in size is seen when both G-block and mucus are both present.

3.3 Multiple Particle Tracking (MPT)

3.3.1 Optimizing mucin concentration

MPT was performed on the carboxyl particles in 30 mg/mL, 45 mg/mL, 60 mg/mL and 120 mg/mL Sigma mucin, as in previous work described as physiologically relevant mucin concentrations.(Dawson *et al.*, 2004, Crater and Carrier, 2010, Norris and Sinko, 1997) The mucus itself showed some fluorescent signal, so mucus with no particles was used to eliminate the background effect this had on the imaging. By using a laser intensity of 51 % and a gain on 630, the background fluorescence from the mucus disappeared. All settings can be found in appendix C, and with the same settings the particles was imaged for 20 s.

For Sigma mucin at the concentration 60 mg/mL the particles showed no movement, so the highest mucus concentration would probably not be necessary to test. In the 120 mg/mL the spaces in the mucin network will probably be filled with a very viscous solution made from the components in the mucus. Since the particles do not move in 60 mg/mL, they would most probably not move in the 120 mg/mL Sigma mucin either. The 30 mg/mL, 45 mg/mL and 60 mg/mL samples were tested and ± 100 trajectories for each mucus concentration were analyzed to find the concentration best suited for the further analysis of amino- and PEGylated particles. As seen in figure 3.3.1-1A the averaged mean square displacement, <MSD> for the 30 mg/mL showed the steepest slope, and the most unhindered diffusion. Both the 45 mg/mL and 60 mg/mL gave rather flat lines, and a more hindered diffusion. The same is also concluded from B, where the $<D_{eff}>$ for 30 mg/mL gave a flatter curve than the two higher concentrations. This result led to the decision that further measurements would be done in 30 mg/mL Sigma mucin.

The fall at the end of each curve, was also investigated, to determine if there was actually something that hindered the particles from diffusing at these timescales, or if it came as a result of the fact that not all trajectories lasted for the entire timescale. Particles which move a lot will be difficult to track throughout the entire timescale, and the trajectories showing least mobility are in this way unintentionally overrepresented at the longest timescales. Movies were captured over longer timescales (40 s), and analyzed in the same manner. The result from this is shown in figure 3.3.1-2. This figure shows that the dips do come at the longest timescales, and not at the same timescale point as in figure 3.3.1-1. The fact that not all trajectories last for the entire

timescale indicates that the particles diffuse out of the focus plane, providing additional evidence for diffusion in the matrix.

It was decided that MPT for aminated- and PEGylated particles should be performed in 30 mg/mL Sigma mucin since carboxyl particles in this concentration showed good mobility. To actually be able to compare the different particle surfaces it was desirable that the particles showed some movement, so not every particle is hindered by a too dense mucus network and appear immobile.

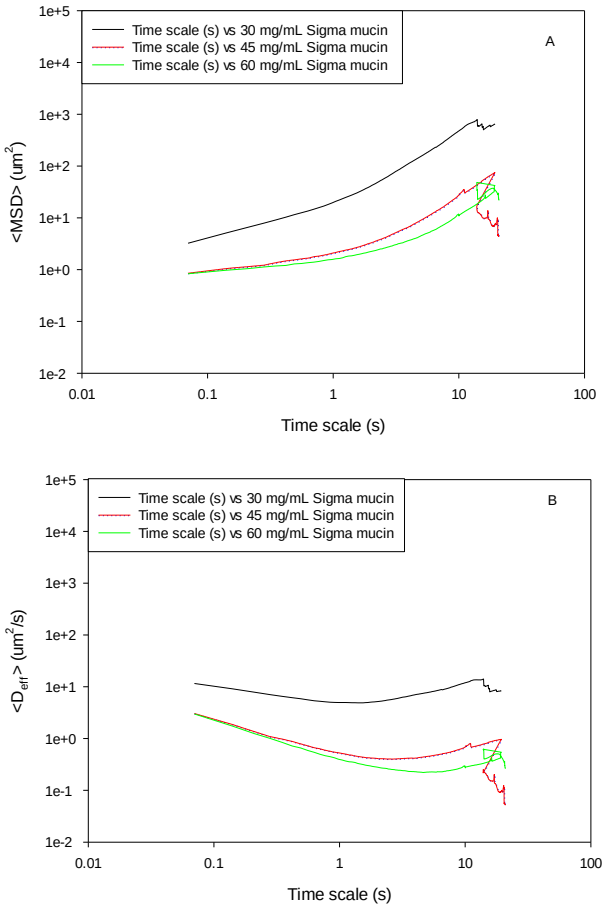

Figure 3.3.1-1 Transport rates of COOH particles in different mucus concentrations. (A) Averaged mean square displacements (<MSD>) plotted against time scale, and (B) effective diffusivities plotted against time scale. Data represents averages from n ~ 100 trajectories for each mucus concentration. Both A and B shows that the particles moves most in the most diluted mucus concentration (30 mg/mL, black lines).

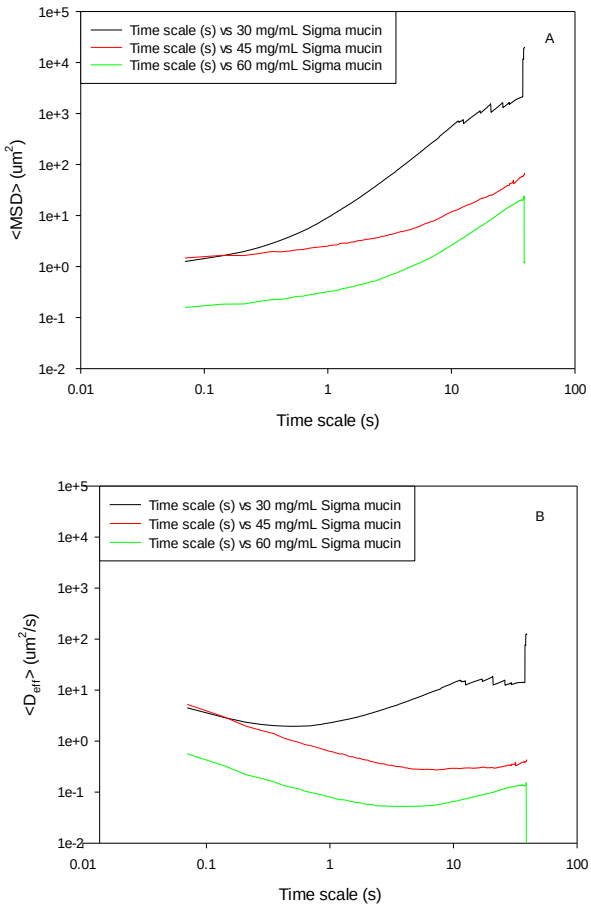

Figure 3.3.1-2. Trajectories for n~100 COOH particles tracked in different mucus concentrations for a longer time interval (40 s) than the trajectories followed in figure 3.3.1-1. This shows that inconsistencies seen always come at the end of each measurement, and not at a specific timescale point.

3.3.2 MPT with G-block

Figures 3.3.2 presents the results from n~100 trajectories of carboxyl, amine and PEGylated particles in Sigma mucin (30 mg/mL) on the top line, and the results from n~100 trajectories of particles in G-block (0.05 mg/mL) *and* Sigma mucin (30 mg/mL) on the bottom line. Their diffusions were analyzed to get mean squared displacement curves, <MSD>, and effective diffusivities curves, $<D_{eff}>$.

3.3.2.1 Diffusion of carboxyl particles

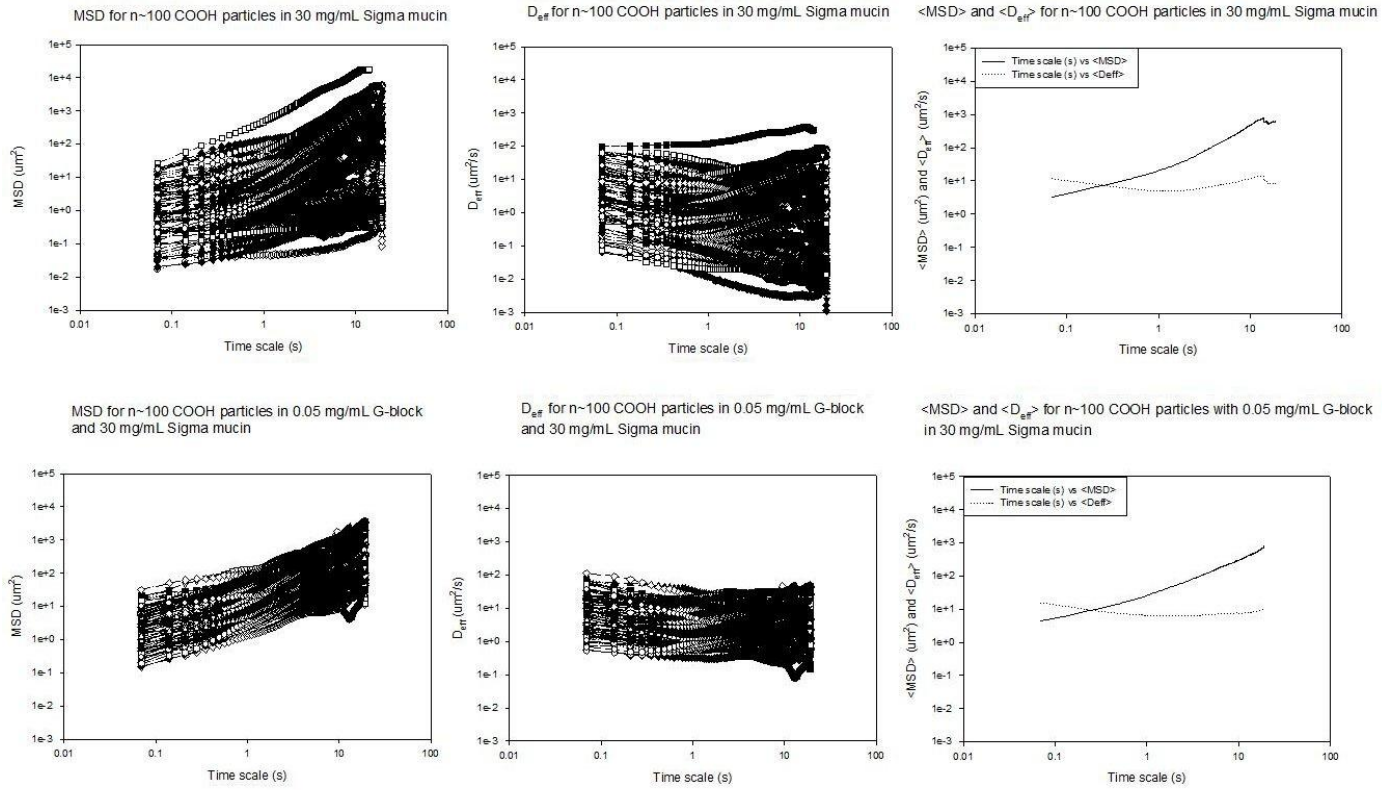

Figure 3.3.2.1-1. The figure shows MSD, D_{eff} and normalized <MSD> and $<D_{eff}>$ for carboxyl particles in 30 mg/mL Sigma mucin (above), and carboxyl particles with 0.05 mg/mL G-block in 30 mg/mL Sigma mucin (below).

When studying the above row on figure 3.3.2.1-1 there are at least two different populations in the graph. In the MSD graph, one shows a relatively constant MSD with time, and one shows

MSD with a steeper increase with time. This tendency is also visible in the D_{eff}-curves where one population is relatively constant and the other decrease with time, indicating subdiffusive transport. In figure 3.3.2.1-2 the two extremes are shown both as D_{eff} and MSD-curves. This clearly shows that there are different modes of transport for particles within the same sample. As classified by Suh (2004) the D_{eff}-curves will show diffusive transport as constant D_{eff} values and subdiffusive transport as D_{eff} values decreasing with time. It is therefore clear that we observe both transport modes in this sample.

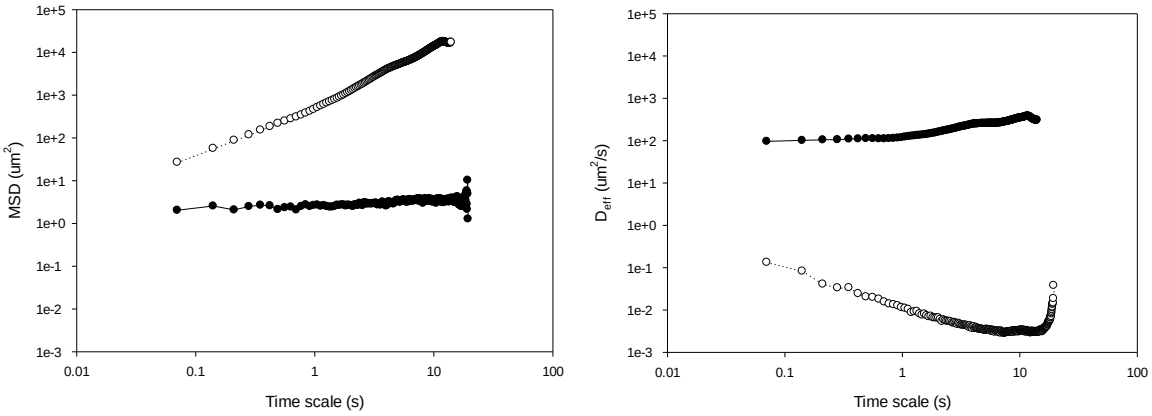

Figure 3.3.2.1-2. The extremities from figure 3.3.2.1-1 extracted to show the differences in mobility within the sample. Flat D_{eff}-curves describe diffusive mobility, while decreasing D_{eff}-curves are typical for particles showing subdiffusive mobility.

After the addition of G-blocks to the particles, the population is more homogenous, all trajectories showing more similar values for MSD and D_{eff}. This may also be stated as the carboxyl particles in G-block show more compact graphs, with less spreading. To investigate this further the normalized particle MSDs, as presented by Crater and Carrier (2010) were studied for particles with and without G-block at timescale $\tau = 0.14$ and $\tau = 14.0$, figure 3.3.2.1-3. This show that the majority of particles MSDs are lower than the ensemble average and that there is a small amount of rapidly moving particles largely affecting the average. When adding G-blocks (c and d), there become fewer of these particles, and the amount of particles with very low MSDs decrease.

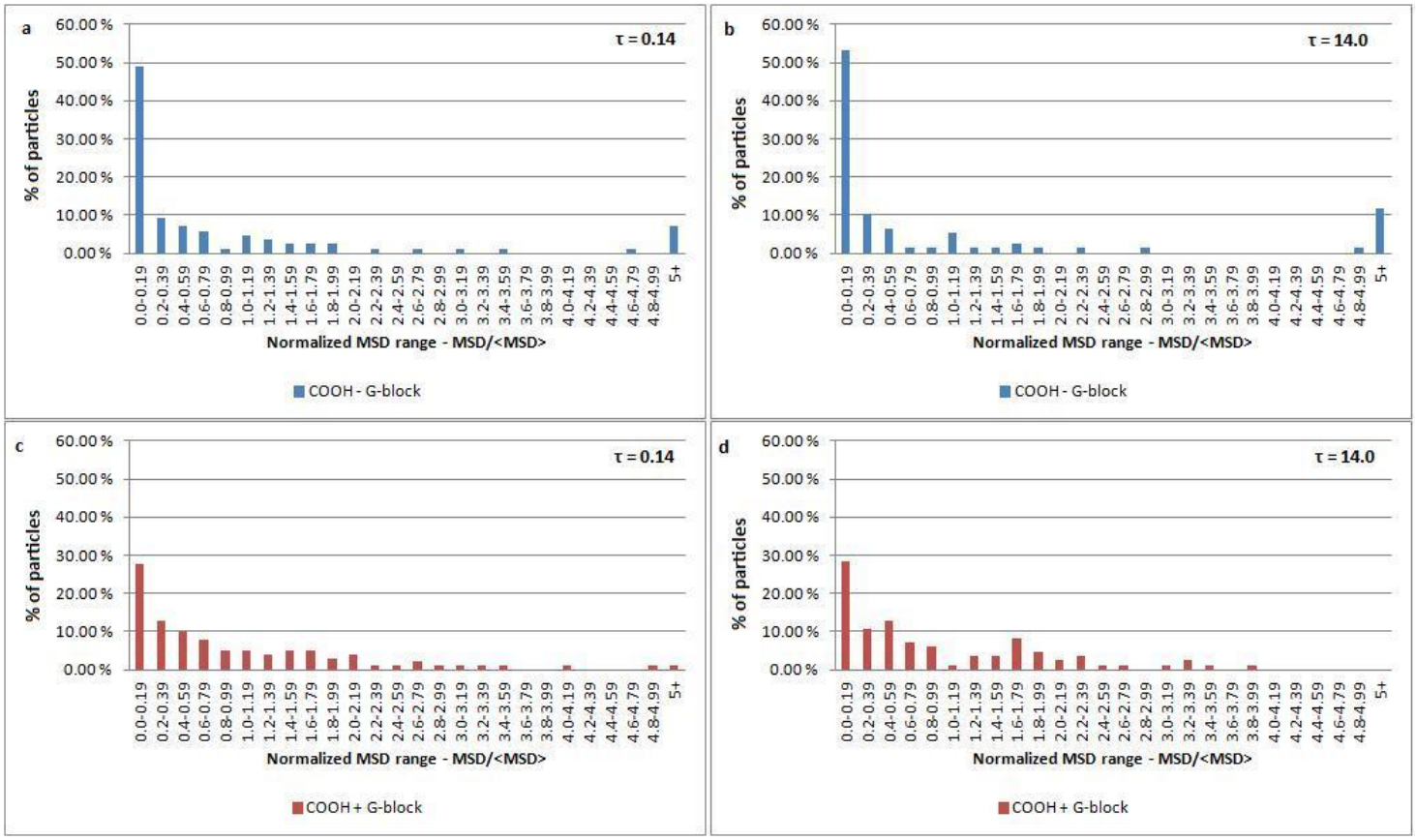

Figure 3.3.2.1-3. Normalized MSD distributions (MSD/<MSD>), for carboxyl particles without (a and b) and with (c and d) G-block at τ = 0.14 (a and c) and at τ = 14.0 (b and d). The graph shows how G-blocks contribute to a more homogenous distribution, more centered around the average value. It also visualizes that particles showing very high or very low MSDs are reduced in number by the addition of G-blocks.

For longer timescales the same is seen (b and d). The amount of particles in the outer ranges is decreased by the addition of G-blocks, and actually there are no particles with very high MSDs at long timescales (figure 3.3.2.1-3d). Crater and Carrier, presented in their study of barrier properties of gastrointestinal mucus to nanoparticles, that the same carboxyl particles from Invitrogen showed a higher percentage of mobile particles at short timescales in the Sigma mucin. This difference in mobility may be due to the use of different salts in the Sigma mucin preparation.

3.3.2.2 Diffusion of amine particles

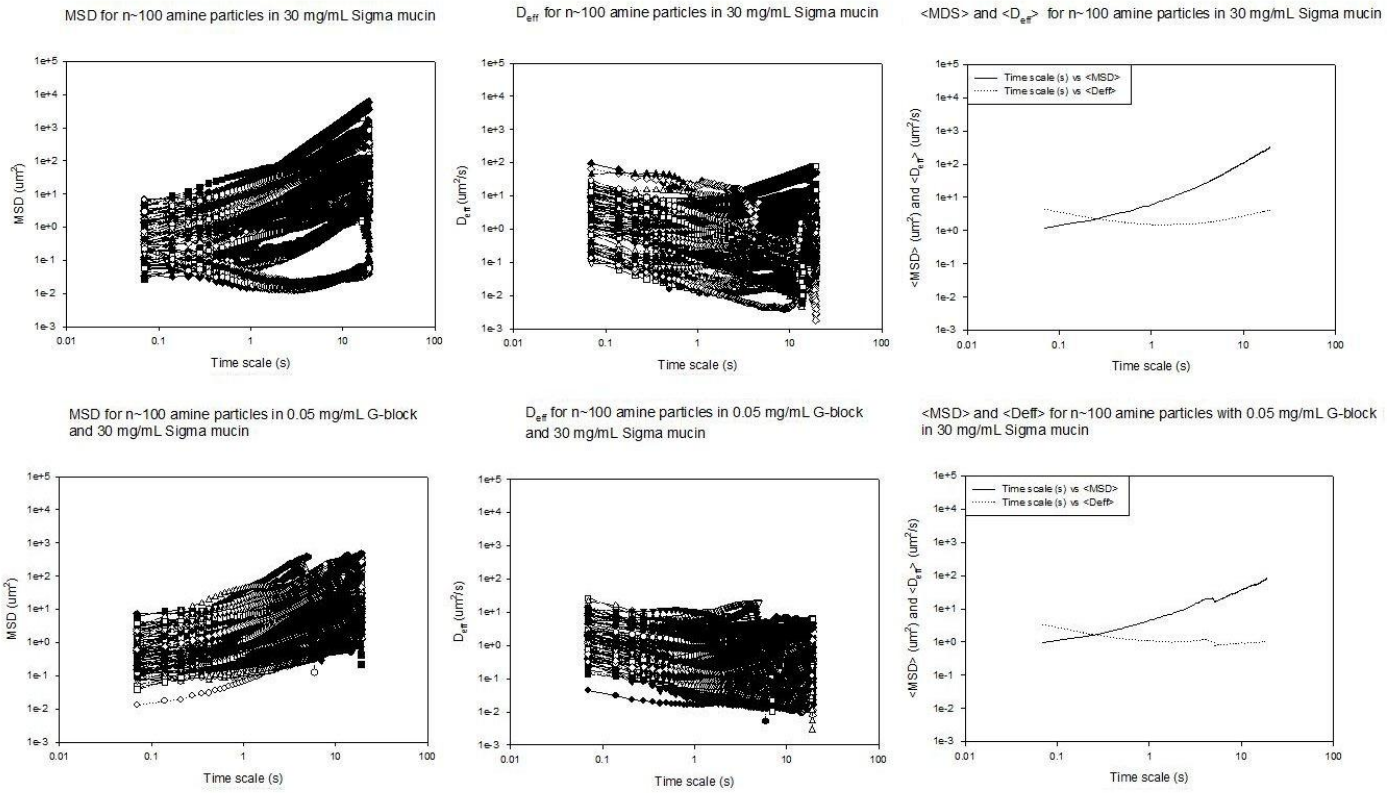

Figure 3.3.2.2-1. The figure shows MSD, D_{eff} and normalized <MSD> and <D_{eff}> for amine particls in 30 mg/mL Sigma mucin (above), and amine particles with 0.05 mg/mL G-block in 30 mg/mL Sigma mucin (below).

Amine particles was tracked and analyzed in the same way as the carboxyl particles and the graphs for MSD and D_{eff} is given in figure 3.3.2.2-1. When studying this figure it is clear that also here there are multiple populations for the particles without G-block. Some MSD curves are flat, and some show steeper curves. In the D_{eff} curves some show active transport. This is not possible in a mucus matrix. The particles could be attached to the mucins and move with them, but if this was the case these movements would also represent diffusion, as mucins would only move with Brownian motion. One possibility may be that the heat induced by the laser on the confocal microscope cause some thermal movement in the sample. Another explanation may be that the entire sample was drifting in one direction, a theory that might be supported by the MSD lines being very straight and constant. The drifting may be due to the sample settling from a non horizontal position. Due to the uncertainty concerning these trajectories and the fact that the

movements are not naturally possible in the system, the trajectories concerned are excluded from further analysis. These measurements would only increase the error in the <MSD> and $<D_{eff}>$. The curves without these trajectories are shown in figure 3.3.2.2-2, here the graphs for the particles with G-block is also shown again just for the convenience when comparing the results.

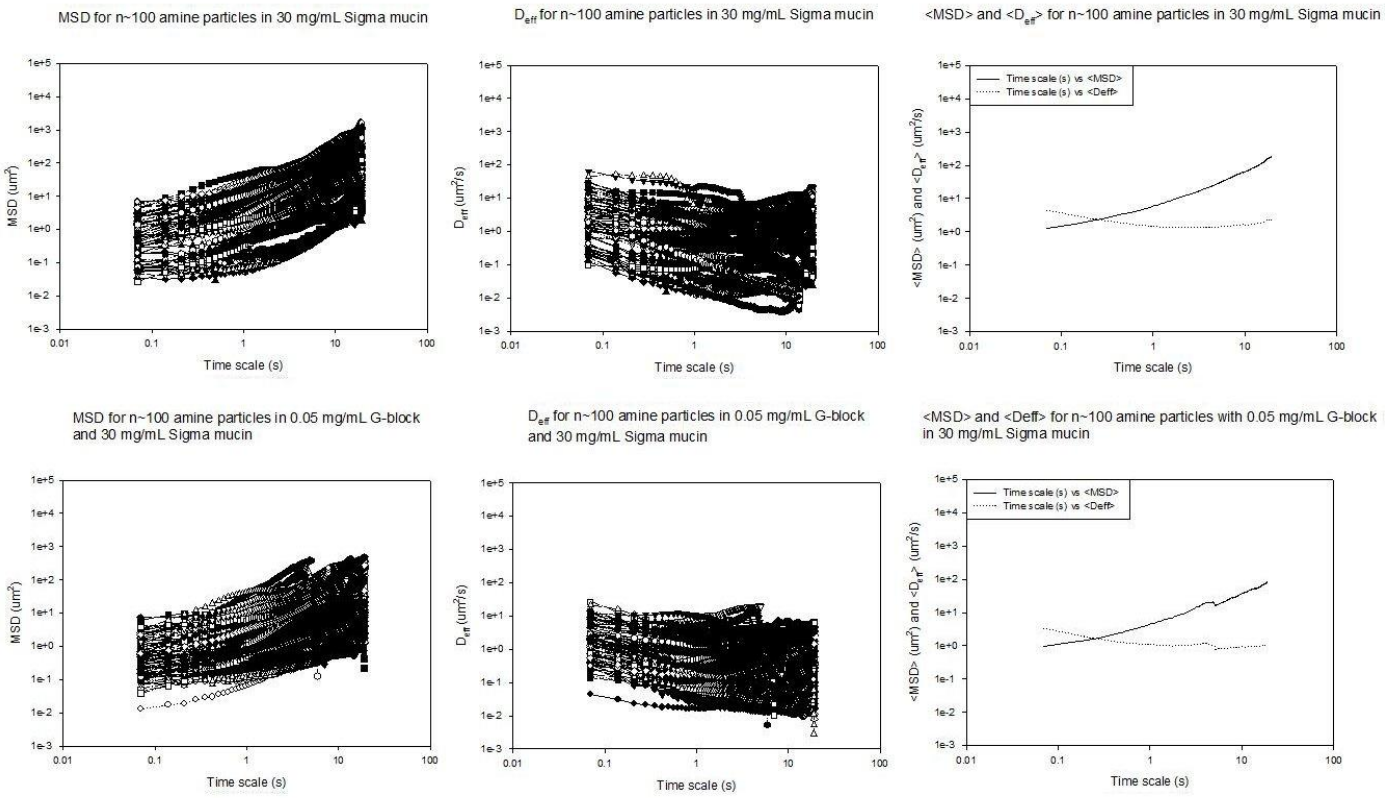

Figure 3.3.2.2-2. The figure shows MSD, D_{eff} and normalized <MSD> and $<D_{eff}>$ for amine particles in 30 mg/mL Sigma mucin (above) after the removal of trajectories showing active transport. The lower row show amine particles with 0.05 mg/mL G-block in 30 mg/mL Sigma mucin as in figure 3.3.2.2-1.

As seen for the carboxyl particles, the addition of G-blocks makes the individual particle trajectories of the amine particles show more homogenous particle mobility. Figure 3.3.2.2-3 shows that more particles have MSDs closer to the average value after the addition of G-blocks, and that the amount of particles with large MSDs, are significantly reduced, contributing to the more homogenous distribution.

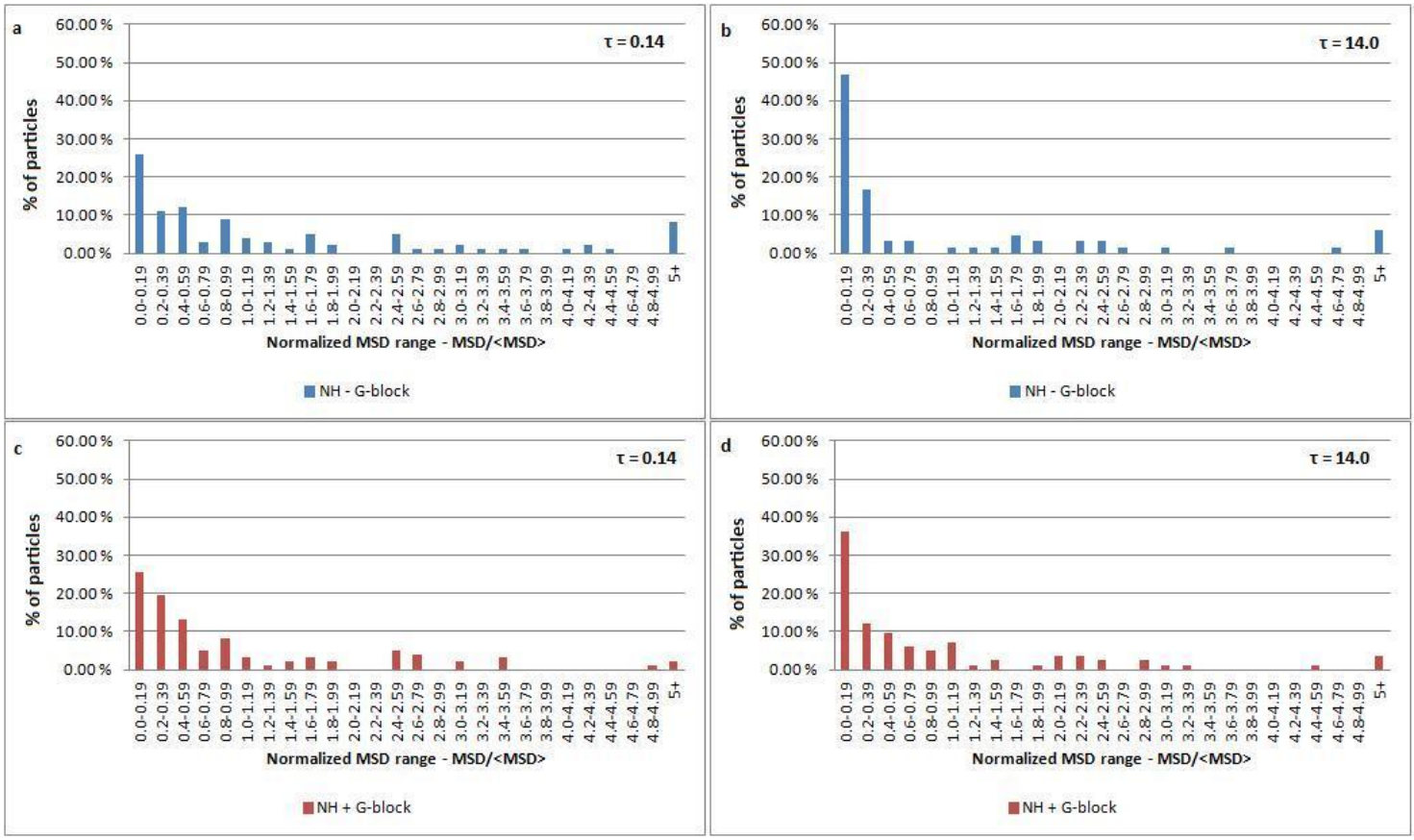

Figure 3.3.2.2-3. Normalized MSD distributions (MDS/<MSD>), for amine particles without (a and b) and with (c and d) G-blocks at τ = 0.14 (a and c) and at τ = 14.0 (b and d). The figure shows that the addition of G-blocks decrease the amount of particles showing very high and very low MSDs, leading the distributions to become more homogenous.

3.3.2.3 Diffusion of PEG covered particles

Figure 3.3.2.3-1, shows that there are many populations also among the PEGylated particles when they are tracked through Sigma mucin. A few particles show flat MSD curves, and there is a large variation in the MSD values at the same timeframes. When G-block was added the trajectories once again showed more homogenous particle mobility distribution, decreasing the difference between the MSD values. Some trajectories showed active transport, and because this is not possible in this system as discussed above, these trajectories were excluded from the analysis, and the new edited graphs are showed in the lower row in figure 3.3.2.3-2.

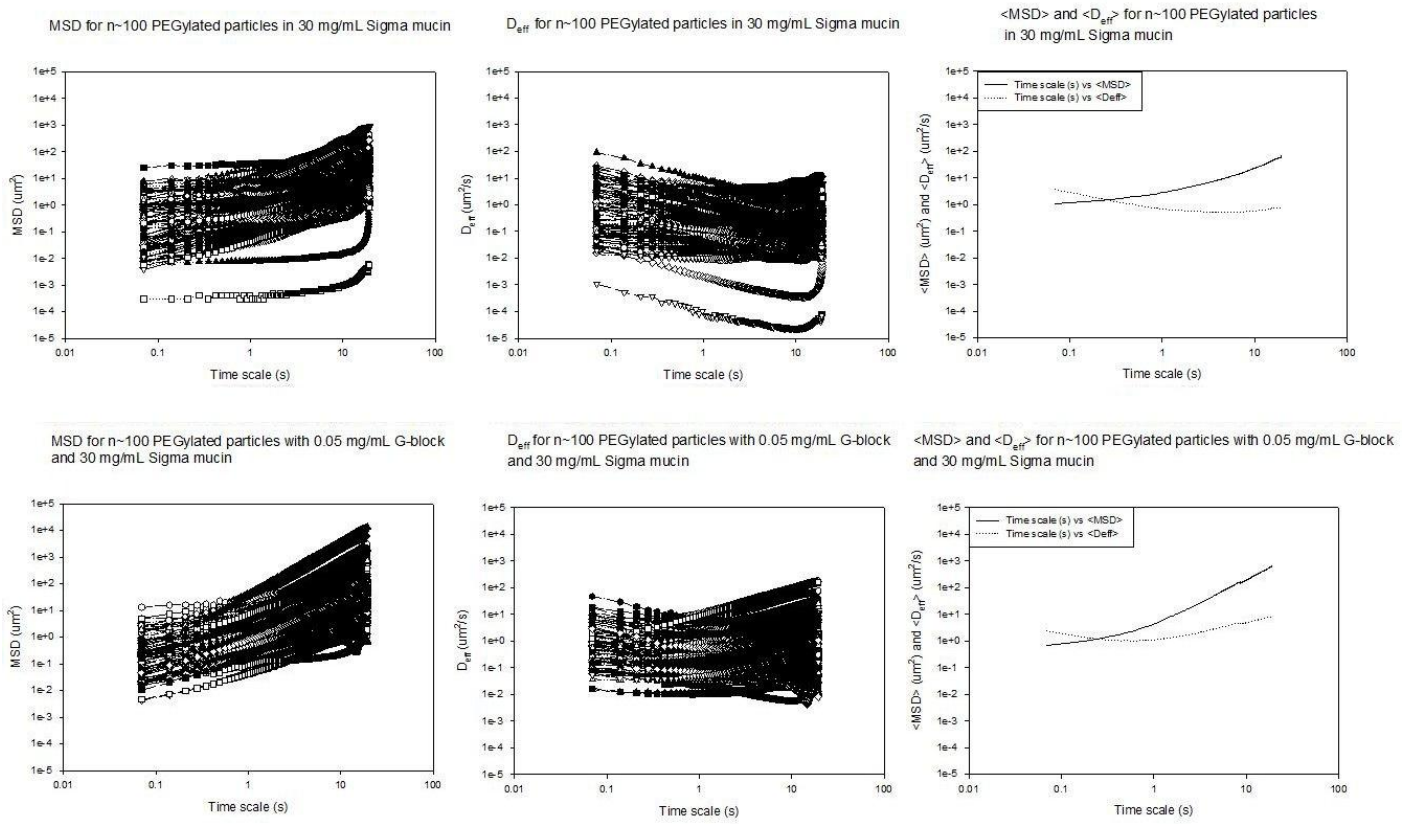

Figure 3.3.2.3-1. The figure shows MSD, D_{eff} and normalized <MSD> and <D_{eff}> for n~100 PEGylated particles in 30 mg/mL Sigma mucin (above), and PEGylated particles with 0.05 mg/mL G-block in 30 mg/mL Sigma mucin (below).

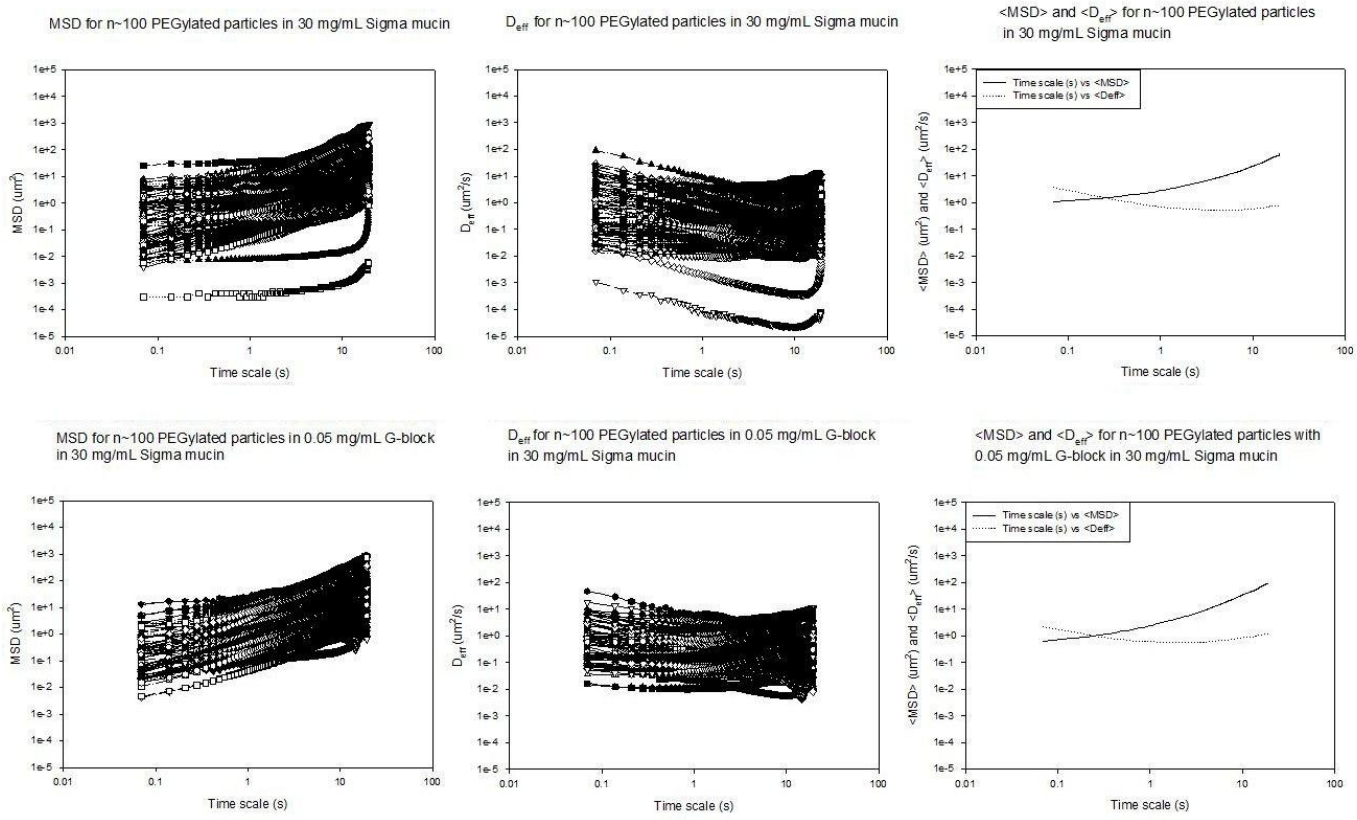

Figure 3.3.2.3-2. The figure shows MSD, D_{eff} and normalized <MSD> and <D_{eff}> for PEGylated particles in 30 mg/mL Sigma mucin (above) as in figure 3.3.2.3-1.The lower row show PEGylated particles with 0.05 mg/mL G-block in 30 mg/mL Sigma mucin after the removal of trajectories showing active transport.

A homogeneity induced by G-blocks is not as easily seen for these particles in the MSD or D_{eff} graphs, but it is visible that the extremities of trajectories disappear by the addition of G-blocks. When investigating the normalized MSDs in figure 3.3.2.3-3 a shift towards a more homogenous distribution is still visible. The amount of particles showing very low MSDs is reduced, and the amount of particles showing normalized MSDs closer to 1 is increased.

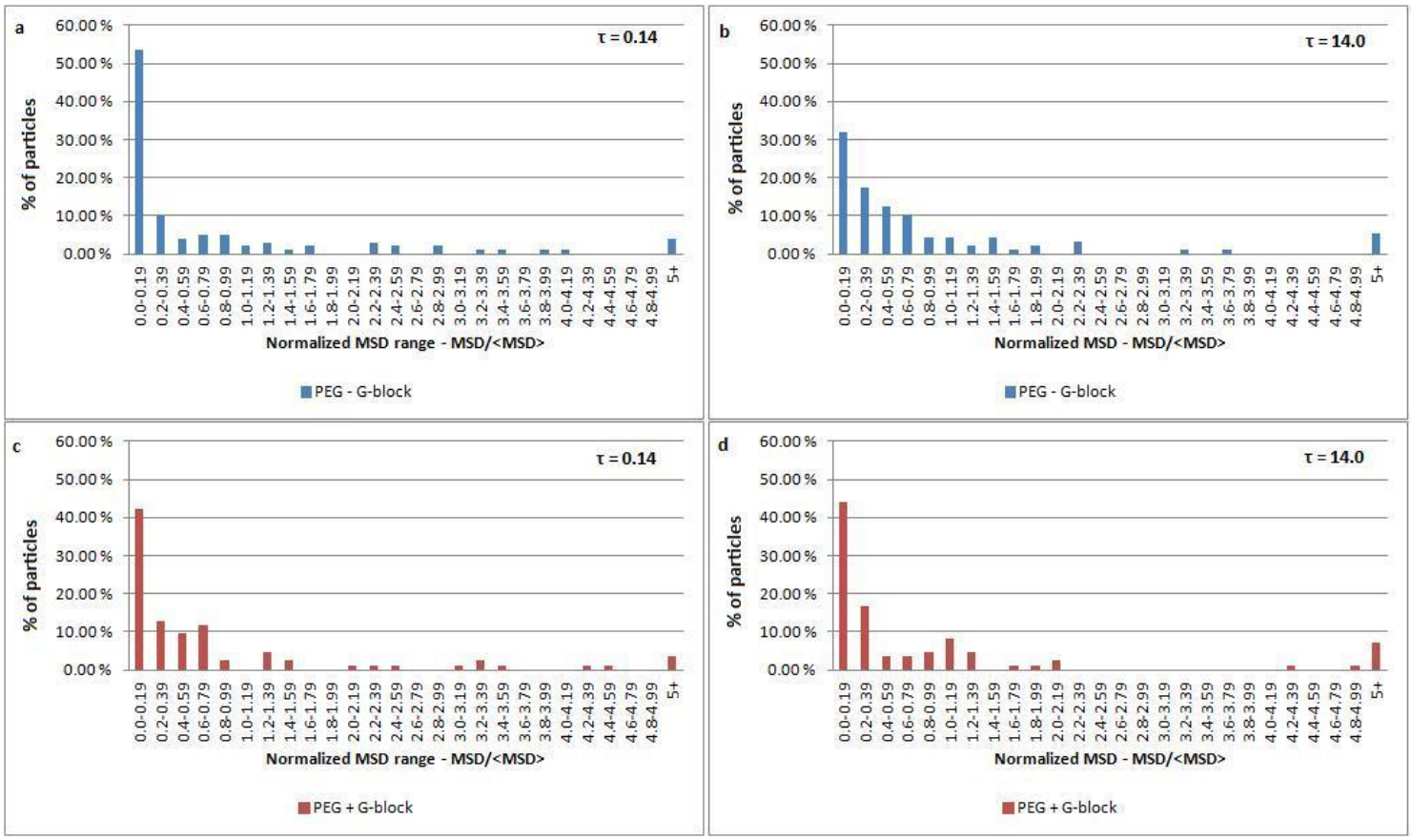

Figure 3.3.2.3-3. Normalized MSD distributions (MDS/<MSD>), for PEGylated particles without (a and b) and with (c and d) G-blocks at τ = 0.14 (a and c) and at τ = 14.0 (b and d). The figure shows that the addition of G-blocks decreases the amount of particles showing very low MSDs, and that the distributions become more homogenous.

These experiments show that G-blocks increase the homogeneity among the trajectory distributions for all particle types. Such an increase in the homogeneity of transport rates has also been showed by Dawson by the addition of the rhDNase Pulmozyme to cystic fibrosis (CF) mucus.(Dawson *et al.*, 2003) She explains this increased homogeneity by the hydrolysis of DNA which forms entanglements with mucin glycoproteins and other CF mucus components. By hydrolyzing DNA the networking properties in the CF mucus will be disrupted. This cause the pores in the matrix to collapse and become smaller, possibly filled with more of the shorter polymers, leading to a higher viscosity in the remaining spacings. This means the faster moving particle populations, which diffuse through the pores, meet more resistance and become more hindered. At the same time particles that were originally held by mucin-DNA aggregates can be

released from their positions and move more freely. In this way both the fastest and the slowest moving particles are affected and the distribution becomes more homogenous. Crater and Carrier (2010) also observed a difference in transport heterogeneity between native intestinal pig mucus and pig gastric mucus from Sigma, as used here. They suggest the higher homogeneity seen in Sigma mucin was due to the absence of the large pores (allowing for rapid particle transport) and non-mucin components increasing the number of possible interactions between particles and the environment (making particles immobile). Compared to native healthy mucus, CF mucus is much more degraded and contains more non-mucin components. In the lungs mucus stasis means nothing is cleansed from this matrix and cellular debris stick to it together with enzymes, which degrade many of the large polymers into shorter polymers further increasing the viscosity. In this way CF mucus is similar to Sigma mucin. It is possible that the way Pulmozyme changes the microstructure of the CF mucus could be compared to how G-blocks act on the Sigma mucin. The G-blocks have shown to change the structure in pig gastric mucin (figure 1.6-3), and it is reasonable to assume that they would have a similar effect on Sigma mucin. The Sigma mucin matrix would most probably consist of different regions with different amounts of structure. G-blocks would probably interact with the regions with structure, making these parts less cross linked, and more similar to the less structured regions. In this way G-blocks could make the pores in the matrix become smaller and filled with more viscous material, causing faster moving particles to slow down, and also allowing for particles previously captured and immobile to be liberated and more mobile.

3.4 Effect of time on diffusion

For all particle types it seems a common trend that they become more diffusive with time, the D_{eff} curves showing an increase towards longer timescales. To investigate this the particles transport mode was determined by the classifications from part 1.7.2. Since the curves obtained were not linear the tangent at the two points $\tau = 0.14$ s ($\Delta\tau$ between 0.14 s – 1.4 s) and $\tau = 14.0$ s ($\Delta\tau$ between 14.0 s -15.4 s) was chosen, as they were points at each side of the bend of the curve. The distributions are showed in figure 3.4-1. At $\tau = 0.14$ s average α-values was 0.4299, 0.2841 and 0.5798 for carboxyl-, amine- and PEG-particles respectively, for particles without G-block. This indicates that all particle types show subdiffusive transport, with at least 40 % of the particles for all three particle types displaying subdiffusive transport at this timescale in figure 3.4-1.

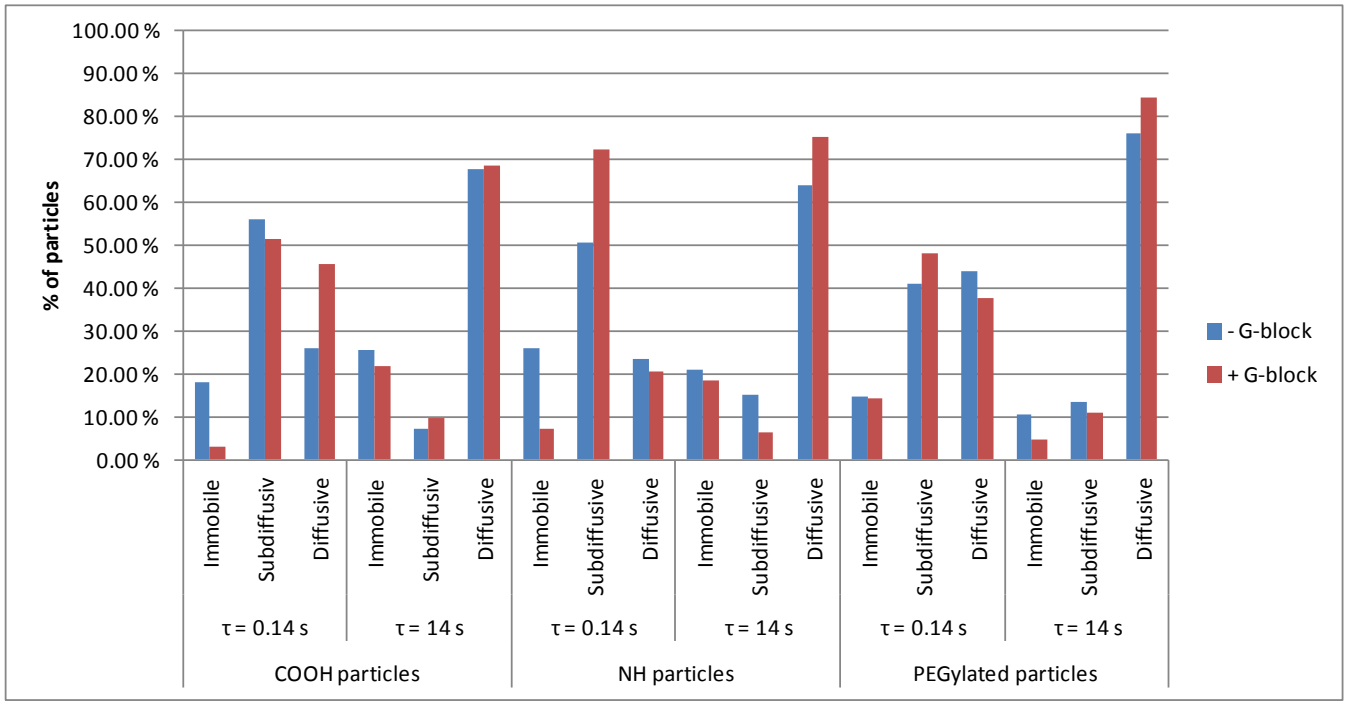

Figure 3.4-1. The figure shows the comparison of particle mode distributions between carboxyl-, amine- and PEGylated particles at two time scales ($\tau = 0.14$ s and $\tau = 14.0$ s). The classifications are based on the anomalous exponent α, being > 0.9 for diffusing particles between 0.2 and 0.9 for subdiffusive particles and < 0.2 for immobile particles.

The α-values also show that the amine particles were hindered the most by particle-mucus interactions. When studying figure 3.4-1, the same is seen as more than 76 % of all amine particles show immobile or subdiffusive mobility at timescales $\tau = 0.14$ s. Conversely the

PEGylated particles had the highest α-value and also the highest percentage of diffusing particles at the same time scale. At longer time scales (τ = 14.0 s) the average α-values for particles without G-blocks was 1.1229, 1.4680 and 1.4030 for carboxyl-, amine- and PEG particles respectively. This indicates that all particle types show diffusive transport at this time scale. This is consistent with all particle types showing at least 60 % of particles with diffusive mobility at longer timescales, both with and without G-block, in figure 3.4-1. That particles seem more mobile at longer time scales has also been showed by Crater and Carrier (2010) and Dawson (2004). They propose this may indicate that the diffusing particles adhere transiently to mucin fibers or get trapped in the mucin network, and that they at higher timescales manage to escape their obstructions. Saxton and Jacobson (1997) describes how most experiments show a change in transport mode at longer time scales, and that if these transitions are real they might represent the entry of particles into new microdomains. Particle transport through complex matrixes can be described with three different diffusivities: microscopic, mesoscopic and macroscopic (figure 3.4-2). Microscopic diffusions (3.4-2A) are based on the particles being small enough to move within the microdomains of the matrix. This diffusion reflects the viscosity within these microdomains more than the bulk-fluid. In mesoscopic diffusion (figure 3.4-2B) the particles are almost as large as the microdomains, as also mentioned in 1.7.2. At early timescales these particles may seem hindered, while they at longer timescales may seem unhindered as they move between microdomains.(Suh *et al.*, 2005) These particles often show biphasic behavior. This is seen in D_{eff}-curves as a decreasing line at short time scales who approach a constant at longer time scales (figure 1.7.2-2).(Saxton, 1994)

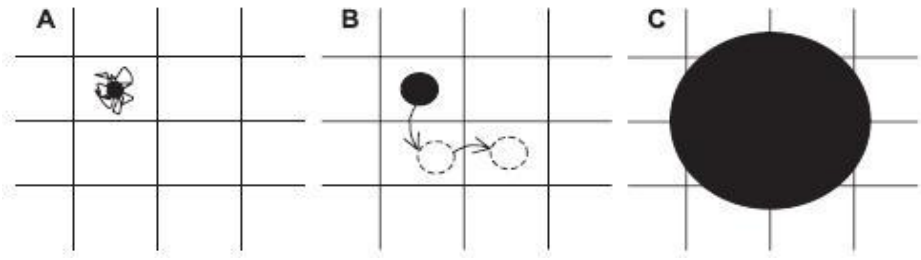

Figure 3.4-2. Three different diffusivities describing particle transport in complex environments. The length scale and the timescale is important when determining what diffusion one is dealing with. A) microscopic diffusion, B) mesoscopic diffusion and C) macroscopic diffusion. From (Suh et al., 2005)

In macroscopic diffusion particles are significantly larger than the microdomains (figure 3.4-2C), and the diffusion is tested in the bulk fluid.(Suh *et al.*, 2005) These characterizations indicate that time scale and length scale is important for the diffusion characterization. It also indicates that what is studied here most probably is mesoscopic diffusion, as the $<D_{eff}>$ curves obtained seem to decrease towards a constant value at longer time scales.

The most profound effect caused by G-blocks is seen for the carboxyl- and amine particles at short timescales (for $\tau = 0.14$ in figure 3.4-1). They both show a decrease in the amount of immobile particles by addition of G-blocks. For the carboxyl particles the amount of diffusive particles is increased, while for the amine particles the amount of subdiffusive particles is increased. For the amine particles this is also consistent with the data from the Zeta Sizer, which indicated that G-blocks could reduce the interactions with matrix components.

3.5 Ensemble <MSD> and <Deff>

The individual particle trajectories were analyzed above and ensemble MSD averages, <MSD> (figure 3.5-1a) and effective diffusivities, $<D_{eff}>$ (figure 3.5-1b) was compared for all three particle types in 30 mg/mL Sigma mucin.

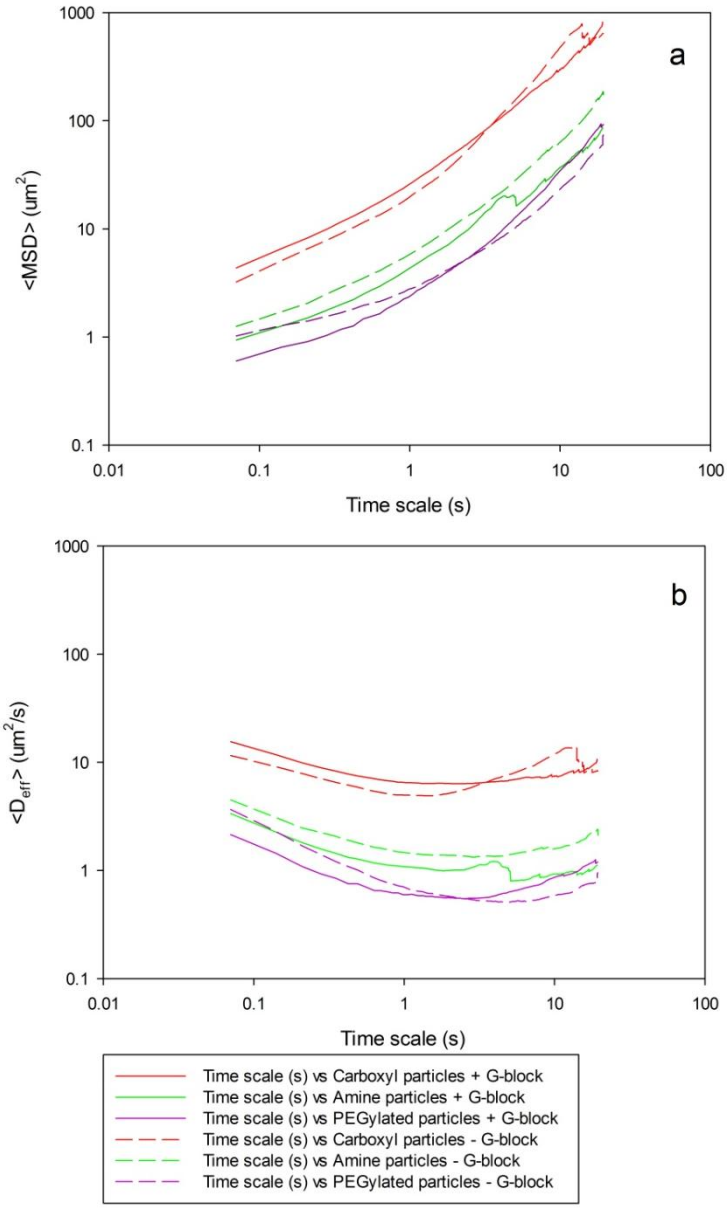

Figure 3.5-1. The <MSD> and $<D_{eff}>$ for all particle types in 30 mg/mL Sigma mucin. Carboxyl particles are seen in red, amine particles in green and PEGylated particles in purple. Samples without G-blocks are represented as dotted lines.

As already seen the G-blocks alter the particle trajectories to show a more homogenous distribution. When studying figure 3.5-1 it is clear that the mean averages are not significantly changed by the addition of G-blocks. The same effect was observed by Dawson (2003); the rhDNase they used made the distribution more homogenous, but the average rates were not affected. From figure 3.5-1 it can be said that the different particles show different diffusion properties. This indicates that the surface structures of the diffusing particles are important. Carboxyl particles show a better mobility than amine particles. It is difficult to compare the PEGylated particles in this analogy since they are so much larger in size. Others have also shown that carboxyl particles from the same producer have a better mobility than amine particles from the same producer in Sigma mucin (Crater and Carrier, 2010), but it has also been shown that the same particles in cystic fibrosis mucus give the opposite results, with amine particles showing the highest transport rate.(Dawson *et al.*, 2003) They explain this by their amine particles having a more neutral charge, and thereby reduced adhesivity towards the CF mucus. Also the amine particles in this thesis were more neutrally charged than the carboxyl particles, but this did not lead to a higher average transport rate. It seems more probable that cationic or near neutral amine particles will be attracted to negatively charged mucin fibers, inhibiting particle diffusion. And that negatively charged carboxyl particles will experience electrostatic repulsive forces from the mucin fibers and by this become more mucoinert, and not be hindered to the same extent. The differences seen from the study of Dawson (2003) and here is most likely due to the difference in the mucus used, since Crater and Carrier (2010) used the same Sigma mucin as here, and saw the same trends. This again proves the importance of considering the type of mucin one is choosing to work with.

As previously shown G-blocks are known to cause an effect on network structures in native mucus. Since the Sigma mucin used in these experiments consists of smaller mucin fragments, not making up the same compact network as in native mucus (figure 1.2-2), there is a possibility that this effect is not seen to the same extent as by Taylor Nordgård and Draget (2011, 2011). It is also likely that this mucus matrix is more heterogeneous, and by containing less of the framework creating mucins, the pores in the Sigma mucin are less complete and less likely to be formed to the same extent as in native mucus. As discussed previously it is also possible that the addition of G-blocks change the small amount of structure in the Sigma mucin matrix so that the pores mentioned by and Carrier and Crater (2010) are less likely to be formed to the same amount.

It was originally hypothesized that changes in surface interactions between particles and mucus matrix components would cause changes in particle mobility in the matrix. According to the size and ζ-potential measurements the amine particles with G-blocks was thought to show the higher mobility through mucus, since these particles became smaller and less charged in Sigma mucin and G-block than in Sigma mucin alone. When studying the MPT data this was not the case. This may have two explanations: The interactions between surface structures and mucins are unimportant or, the mucins responsible for the interactions holding the amine particles back were absent in the Zeta Sizer measurements. According to explanation number one carboxyl and amine particles should show the same diffusions through mucus, since they have the same size and the charge wouldn't have an effect. This is unlikely to hold true since the diffusion of carboxyl and amine particles was seen to be different. Others have also been studying this, obtaining different diffusions for the two, the same results as presented here. (Crater and Carrier, 2010) When measuring with the Zeta Sizer the Sigma mucin was much more dilute and filtered, to meet the criterions of the machine. There is a possibility that the larger mucin components filtered out in this procedure are important components of the mucin matrix studied in the MPT. The two Sigma mucin types that are created by this dilution and filtration actually may not be comparable, since the Zeta Sizer-data may not reflect the interactions with large mucin polymers, but only the interactions with the non-mucin components and the smallest mucin polymers.

3.6 Summary and future prospective

The effect of Sigma mucin on three different particle surfaces (approx. 200 nm) was investigated by dynamic light scattering. The results showed that Sigma mucin tend to aggregate on to all surfaces but to a different extent. The most aggregation was seen on positively charged amine particles. G-blocks were shown to diminish the amount of Sigma mucin components adsorbing on to these positively charged particles but not for the other particles investigated.

By multiple particle tracking it has been showed that G-blocks make the diffusion through Sigma mucin more homogenous. It has also been showed that the average diffusion rates are not changed, and that the surface charge of the diffusing particles seems to be the determining factor for diffusion. The effect of G-blocks for improved diffusion was relatively small in this matrix, probably due to the lack of networking elements in this mucin type compared to "more natural" mucus types.

From this it would be interesting to further investigate the diffusions of the particles with G-blocks in other mucus matrixes, such as native mucus and cystic fibrosis mucus. This would give more knowledge on how the findings discovered here correlate to the "real" matrixes. The study of interactions between components in these systems and particles could most probably be done in a Master Sizer instead of in a Zeta Sizer, not giving the same restrictions concerning the light scattering. It would also be exiting to investigate the sequence of G-block addition, and whether this is of any importance for the diffusions. Adding the G-blocks to the mucus matrix *before* applying the particles could lead to different results than obtained here as the G-blocks could open up the network, keeping it open for the particles. It would also be interesting to apply the particles to one restricted side of the mucus, not stirring them in as done here. This could allow us to study how the particles will diffuse into the mucus, and whether this entry into the mucus layer is changed by adding G-blocks. It would be interesting to correlate these findings with the nanoparticle uptake in the cell studies currently being performed by Taylor Nordgård. In addition it would of course have been desirable to do the PEGylation again, to obtain smaller, more densely covered particles, more suited for comparison with the other particles investigated.

4 Conclusion

Sigma mucin will aggregate on positive, negative and neutral surfaces but to a different amount. The largest size increase is seen on positive particles. For positive particles addition of G-blocks inhibits Sigma mucin aggregation. It is concluded that the interactions observed between particles and Sigma mucin components does not correlate with the observed mobility of the nanoparticles in the Sigma mucin matrix. What seems to determine the interactions with Sigma mucin matrix components is the surface structure of the original particle. G-blocks make diffusion trajectories show a more homogenous distribution, but the mean diffusion rates still remain unchanged and G-blocks does not show a huge effect on this system. This is most probably caused by the lack of large structuring mucin components in the Sigma mucin compared to native pig gastric mucin.

References

ALLEN, A. 1983. Mucus — a protective secretion of complexity. *Trends in Biochemical Sciences,* 8**,** 169-173.

ALLEN, A. & GARNER, A. 1980. Mucus and bicarbonate secretion in the stomach and their possible role in mucosal protection. *Gut,* 21**,** 249-262.

BANSIL, R., STANLEY, H. E. & LAMONT, J. T. 1995. MUCIN BIOPHYSICS. *Annual Review of Physiology,* 57**,** 635-657.

BANSIL, R. & TURNER, B. S. 2006. Mucin structure, aggregation, physiological functions and biomedical applications. *Current opinion in colloid & interface science,* 11**,** 164-170.

CARLSTEDT, I. & SHEEHAN, J. K. 1989. Structure and macromolecular properties of cervical mucus glycoproteins. *Symposia of the Society for Experimental Biology,* 43**,** 289-316.

CHEMICELL. 2011. *New PEGylation reagents from chemicell* [Online]. Berlin: chemicell GmbH. Available: http://www.chemicell.com/products/peg/index.html [Accessed 14.02. 2012].

CHRISTENSEN, B. E. 2010. Alginat, tillegskompendium. *TBT 4135 Biopolymerkjemi.* NTNU, Gløshaugen: NOBIPOL, NTNU.

CONE, R. A. 2009. Barrier properties of mucus. *Advanced drug delivery reviews,* 61**,** 75-85.

COX, G. 2007. *Optical imaging techniques in cell biology,* Boca Raton, Florida, CRC, Taylor & Francis.

CRATER, J. S. & CARRIER, R. L. 2010. Barrier properties of gastrointestinal mucus to nanoparticle transport. *Macromolecular bioscience,* 10**,** 1473-1483.

CU, Y. & SALTZMAN, W. M. 2009. Drug delivery: Stealth particles give mucus the slip. *Nature Materials,* 8**,** 11-13.

DAWSON, M., KRAULAND, E., WIRTZ, D. & HANES, J. 2004. Transport of polymeric nanoparticle gene carriers in gastric mucus. *Biotechnology progress,* 20**,** 851-857.

DAWSON, M., WIRTZ, D. & HANES, J. 2003. Enhanced Viscoelasticity of Human Cystic Fibrotic Sputum Correlates with Increasing Microheterogeneity in Particle Transport. *Journal of Biological Chemistry,* 278**,** 50393-50401.

DOAK, J., GUPTA, R. K., MANIVANNAN, K., GHOSH, K. & KAHOL, P. K. 2010. Effect of particle size distributions on absorbance spectra of gold nanoparticles. *Physica E: Low-dimensional Systems and Nanostructures,* 42**,** 1605-1609.

DRAGET, K. I. 2011. Oligomers: Just background noise or as functional elements in structured biopolymer systems? *Food Hydrocolloids,* 25**,** 1963-1965.

DRAGET, K. I. & TAYLOR, C. 2011. Chemical, physical and biological properties of alginates and their biomedical implications. *Food Hydrocolloids,* 25**,** 251-256.

ERTESVAG, H., HOIDAL, H. K., HALS, I. K., RIAN, A., DOSETH, B. & VALLA, S. 1995. A family of modular type mannuronan C-5-epimerase genes controls alginate structure in Azotobacter vinelandii. *Mol Microbiol,* 16**,** 719-31.

ERTESVÅG, H., VALLA, S. & SKJÅK-BRÆK, G. 2009. Enzymatic Alginate Modification *In:* REHM, B. H. A. (ed.) *Microbiology Monographs, Alginates: Biology and Applications.* Springer Berlin / Heidelberg.

GIMMESTAD, M., ERTESVÅG, H., HEGGESET, T. M. B., AARSTAD, O., SVANEM, B. I. G. & VALLA, S. 2009. Characterization of Three New Azotobacter vinelandii Alginate Lyases, One of Which Is Involved in Cyst Germination. *Journal of Bacteriology,* 191**,** 4845-4853.

GRASDALEN, H. 1983. High-field, 1H-n.m.r. spectroscopy of alginate: sequential structure and linkage conformations. *Carbohydrate Research,* 118**,** 255-260.

HARRIS, J. M. & CHESS, R. B. 2003. Effect of pegylation on pharmaceuticals. *Nature Reviews Drug Discovery,* 2**,** 214-221.

HARRIS, J. M., MARTIN, N. E. & MODI, M. 2001. Pegylation: A Novel Process for Modifying Pharmacokinetics. *Clinical Pharmacokinetics,* 40**,** 539-551.

HAUG, A., LARSEN, B. & SMIDSROD, O. 1966. A study of the constitution of alginic acid by partial acid hydrolysis. *Acta Chem. Scand,* 20**,** 183-190.

HAUG, A., LARSEN, B. & SMIDSROD, O. 1967. Studies on the Sequence of Uronic Acid Residues in Alginic Acid. *Acta Chem. Scand,* 21**,** 691-704.

HIEMENZ, P. C. & RAJAGOPALAN, R. 1997. *Priciples of Colloid and Surface Chemistry,* Boca Raton, Florida, CRC, Taylor & Francis.

INVITROGEN & MOLECULARPROBES 2004. Working With FluoSpheres Fluorescent Microspheres. Invitrogen.

INVITROGEN & MOLECULARPROBES 2005. FluoSpheres Fluorescent Microspheres. *In:* INVITROGEN (ed.). Invitrogen.

KHANVILKAR, K., DONOVAN, M. D. & FLANAGAN, D. R. 2001. Drug transfer through mucus. *Advanced drug delivery reviews,* 48**,** 173-193.

KING, M. & RUBIN, B. K. 2002. Pharmacological approaches to discovery and development of new mucolytic agents. *Advanced drug delivery reviews,* 54**,** 1475-1490.

LAI, S. K., O'HANLON, D. E., HARROLD, S., MAN, S. T., WANG, Y. Y., CONE, R. & HANES, J. 2007. Rapid transport of large polymeric nanoparticles in fresh undiluted human mucus. *Proceedings of the National Academy of Sciences,* 104**,** 1482-1487.

LAI, S. K., SUK, J. S., PACE, A., WANG, Y. Y., YANG, M., MERT, O., CHEN, J., KIM, J. & HANES, J. 2011. Drug carrier nanoparticles that penetrate human chronic rhinosinusitis mucus. *Biomaterials,* 32**,** 6285-6290.

LAI, S. K., WANG, Y. Y., CONE, R., WIRTZ, D. & HANES, J. 2009c. Altering mucus rheology to "solidify" human mucus at the nanoscale. *PLoS One,* 4**,** 6.

LAI, S. K., WANG, Y. Y. & HANES, J. 2009a. Mucus-penetrating nanoparticles for drug and gene delivery to mucosal tissues. *Advanced drug delivery reviews,* 61**,** 158-171.

LAI, S. K., WANG, Y. Y., WIRTZ, D. & HANES, J. 2009b. Micro-and macrorheology of mucus. *Advanced drug delivery reviews,* 61**,** 86-100.

LENTER, M., GARIDEL, P., PELISEK, J., WAGNER, E. & OGRIS, M. 2004. Stabilized Nonviral Formulations for the Delivery of MCP-1 Gene into Cells of the Vasculoendothelial System. *Pharmaceutical Research,* 21**,** 683-691.

MALVERN 2004. Zetasizer Nano Series User Manual. Worecestershire: Malvern Instruments Ltd.

MALVERN. 2011. *Zetasizer Nano ZS90* [Online]. Malvern instruments. Available: http://www.malvern.com/labeng/products/zetasizer/zetasizer_nano/zetasizer_nano_zs90.htm [Accessed 29.09. 2011].

MAYER, L. & WALKER, A. W. 2005. Development and Physiology of Mucosal Defence: An Introduction. *In:* AL, M. E. (ed.) *Mucosal Immunology.* 3rd ed.: Elsevier.

MISHRA, S., WEBSTER, P. & DAVIS, M. E. 2004. PEGylation significantly affects cellular uptake and intracellular trafficking of non-viral gene delivery particles. *Eur J Cell Biol,* 83**,** 97-111.

NORRIS, D. A. & SINKO, P. J. 1997. Effect of size, surface charge, and hydrophobicity on the translocation of polystyrene microspheres through gastrointestinal mucin. *Journal of Applied Polymer Science,* 63**,** 1481-1492.

OGRIS, M., WALKER, G., BLESSING, T., KIRCHEIS, R., WOLSCHEK, M. & WAGNER, E. 2003. Tumor-targeted gene therapy: strategies for the preparation of ligand–polyethylene glycol–polyethylenimine/DNA complexes. *Journal of Controlled Release,* 91**,** 173-181.

OLMSTED, S. S., PADGETT, J. L., YUDIN, A. I., WHALEY, K. J., MOENCH, T. R. & CONE, R. A. 2001. Diffusion of Macromolecules and Virus-Like Particles in Human Cervical Mucus. *Biophysical journal,* 81**,** 1930-1937.

OTTERLEI, M., OSTGAARD, K., SKJAK-BRAEK, G., SMIDSROD, O., SOON-SHIONG, P. & ESPEVIK, T. 1991. Induction of cytokine production from human monocytes stimulated with alginate. *J Immunother (1991),* 10**,** 286-91.

PATTON, J. S. & BYRON, P. R. 2007. Inhaling medicines: delivering drugs to the body through the lungs. *Nat Rev Drug Discov,* 6**,** 67-74.

PUN, S. H., TACK, F., BELLOCQ, N. C., CHENG, J., GRUBBS, B. H., JENSEN, G. S., DAVIS, M. E., BREWSTER, M., JANICOT, M., JANSSENS, B., FLOREN, W. & BAKKER, A. 2004. Targeted delivery of RNA-cleaving DNA enzyme (DNAzyme) to tumor tissue by transferrin-modified, cyclodextrin-based particles. *Cancer Biol Ther,* 3**,** 641-50.

QURAISHI, M. S., JONES, N. S. & MASON, J. 1998. The rheology of nasal mucus: a review. *Clinical Otolaryngology & Allied Sciences,* 23**,** 403-413.

ROUSSEL, P., LAMBLIN, G., LHERMITTE, M., HOUDRET, N., LAFITTE, J.-J., PERINI, J.-M., KLEIN, A. & SCHARFMAN, A. 1988. The complexity of mucins. *Biochimie,* 70**,** 1471-1482.

SANDERS, N., DE SMEDT, S. C., CHENG, S. H. & DEMEESTER, J. 2002. Pegylated GL67 lipoplexes retain their gene transfection activity after exposure to components of CF mucus. *Gene Therapy,* 9**,** 363-371.

SANDERS, N., RUDOLPH, C., BRAECKMANS, K., DE SMEDT, S. C. & DEMEESTER, J. 2009. Extracellular barriers in respiratory gene therapy. *Advanced drug delivery reviews,* 61**,** 115-127.

SAXTON, M. J. 1994. Anomalous diffusion due to obstacles: a Monte Carlo study. *Biophys J,* 66**,** 394-401.

SAXTON, M. J. & JACOBSON, K. 1997. SINGLE-PARTICLE TRACKING:Applications to Membrane Dynamics. *Annual Review of Biophysics and Biomolecular Structure,* 26**,** 373-399.

SMIDSRØD, O. & MOE, S. T. 1995. *Biopolymerkjemi,* Trondheim, Tapir Forlag.

SMITH, MATTHEW B., KARATEKIN, E., GOHLKE, A., MIZUNO, H., WATANABE, N. & VAVYLONIS, D. 2011. Interactive, Computer-Assisted Tracking of Speckle Trajectories in Fluorescence Microscopy: Application to Actin Polymerization and Membrane Fusion. *Biophysical journal,* 101**,** 1794-1804.

SUH, J., CHOY, K. L., LAI, S. K., SUK, J. S., TANG, B. C., PRABHU, S. & HANES, J. 2007. PEGylation of nanoparticles improves their cytoplasmic transport. *International Journal of Nanomedicine,* 2**,** 735.

SUH, J., DAWSON, M. & HANES, J. 2005. Real-time multiple-particle tracking: applications to drug and gene delivery. *Advanced drug delivery reviews,* 57**,** 63-78.

SUH, J., WIRTZ, D. & HANES, J. 2004. Real-Time Intracellular Transport of Gene Nanocarriers Studied by Multiple Particle Tracking. *Biotechnology progress,* 20**,** 598-602.

SUN, X., ROSSIN, R., TURNER, J. L., BECKER, M. L., JORALEMON, M. J., WELCH, M. J. & WOOLEY, K. L. 2005. An assessment of the effects of shell cross-linked nanoparticle size, core composition, and surface PEGylation on in vivo biodistribution. *Biomacromolecules,* 6**,** 2541-54.

TAYLOR, C. 2001. *The Structure of the Mucus Gel Barrier and the Interactions with Alginates.* Doctor of Philosophy PhD, University of Newcastle upon Tyne.

TAYLOR, C., PEARSON, J. P., DRAGET, K. I., DETTMAR, P. W. & SMIDSRØD, O. 2005. Rheological characterisation of mixed gels of mucin and alginate. *Carbohydrate Polymers,* 59**,** 189-195.

TAYLOR NORDGÅRD, C. & DRAGET, K. I. 2011. Oligosaccharides As Modulators of Rheology in Complex Mucous Systems. *Biomacromolecules,* 12**,** 3084-3090.

WANG, Y. Y., LAI, S. K., SUK, J. S., PACE, A., CONE, R. & HANES, J. 2008. Addressing the PEG mucoadhesivity paradox to engineer nanoparticles that "slip" through the human mucus barrier. *Angewandte Chemie International Edition,* 47**,** 9726-9729.

ZAHR, A. S., DE VILLIERS, M. & PISHKO, M. V. 2005. Encapsulation of drug nanoparticles in self-assembled macromolecular nanoshells. *Langmuir,* 21**,** 403-10.

List of appendixes

CD (enclosed): Raw data

1) Example of confocal videos captured of particles in 30 mg/mL PGM
2) Raw data trajectory .txt files
3) Raw data MPT .txt files
4) Sigmaplot Notebooks containing MSD, D_{eff}, <MSD> and $<D_{eff}>$ values and graphs

Appendix A: Zeta Sizer SOPs

Size SOP

The size measurements were all done with the same SOP, saved as "latex size.sop – Size". The parameters for this SOP are listed in table A1.

Table A1. The parameters set in the SOP used to perform all size measurements on the Zeta Sizer.

Sample	Material: Polystyrene latex		
	RI: 1.590	Absorption: 0.01	
	Dispersant: Water		
	Temperature: 25 °C	Viscosity: 0.8872 cP	RI: 1.330
	Mark-Houwink Parameters: A parameter: 3.4028e+38 K parameter: 3.4028e+38		
	Use dispersant viscosity as sample viscosity		
	Temperature: 25 °C	Calibration time: 0 sec	
	Cell type: ZEN0112 – Low volume disposable sizing cuvette		
Measurements	Measurement Angle: 173 ° Backscatter (NIBS default)		
	Duration: Automatic	Number of measurements: 3	Delay between measurements: 0 sec
	Automatic attenuation selected		
	Analysis model: General purpose		

ζ-potential SOP

All measurements of ζ-potential were done with the same SOP to reduce the risk of introducing errors to the parameters, and to make the work more efficient. The parameters set in the SOP, saved as "Kari zeta", are listed in table A2.

Table A2. The parameters set in the SOP used for all ζ-potential measurements in the Zeta Sizer.

Sample	Material: Polystyrene latex		
	RI: 1.590	Absorption: 0.01	
	Dispersant: Water		
	Temperature: 25 °C	Viscosity: 0.8872 cP	RI: 1.330
	Dielectric constant: 78.5		
	Model: Smoluchowski F (Ka) value: 1.50		
	Use dispersant viscosity as sample viscosity		
	Temperature: 25 °C	Equilibration time: 20 sec	
	Cell type: DTS1060C – Clear disposable zeta cell		
Measurements	Duration: Automatic	Minimum runs: 10	Maximum runs: 100
	Number of measurements: 3	Delay between measurements: 0 sec	
	Automatic attenuation selected		
	Analysis model: General purpose		

Appendix B: PEGylation protocol

This PEGylation protocol was made based on the protocols given by Invitrogen and MolecularProbes (2004) and Suh (2007). The PEGylation was performed on the 18.-19. October 2011. The centrifuge available only had the capacity to do 11 000 rpm, so the centrifugation was done for 50 min each round. Still lots of particles were lost together with the supernatant, so the centrifuge could with benefit have been faster.

In step 1 HyClone DPBS from Thermo Scientific was used. (DPBS 10x liquid, Cat.no.SH30378.02, Lot.no. AVH73876, Bottle no. 00874) In step 2 MES from SIGMA (Lot 111H5623, M-3885) was used to make the MES-buffer, and the pH was adjusted with 0,1 M and 0,2 M HCl to 6,02. At step 6 the pH was adjusted to 6,48. This was regarded as ok, since Invitrogen and MolecularProbes (2004) states that pH 6±0.2 is good.

The EDAC used in step 5 was obtained from VWR. (CAS nr. 25952-53-8, SL305)

After step 11, the pellet was suspended in 5 mL MQ water to obtain the same 2 % particles in suspension as the original particles from Invitrogen.

PEGylation Protocol:

1. Dilute 10 mL PBS buffer: 1 mL of buffersolution to 9 mL water.

2. Make 100 mL MES buffer 50 mM pH 6
Mix 0.976 g MES and some of the water. Adjust the pH to 6 and add the rest of the water to a total volume of 100 mL

3. Dissolve PEG-amine (5 kDa) in 50 mM MES buffer at pH 6.
Add carboxylated nanospheres to a final concentration of 10 mg PEG/mL and 1 % solids/mL.
Want total volume of 10 mL → must have 100 mg PEG. Particle suspension contains 2% solids. Dilute

the particles 1:2.
Add 100 mg PEG to 4.75 mL MES buffer. Then add 5 mL of the 2 % (original) particle solution.
The PEG is in aqueous solution; 400 mg/mL. Uses ¼ mL → 0.25 mL.

4. Incubate at room temperature for 15 min

5. Add EDAC to a concentration of 4 mg/mL. → Add 40 mg = 0.04 g

6. Adjust the pH to 6.5 with dilute NaOH

7. Incubate on orbital shaker at room temperature for 2 hrs

8. Add glycine to a final concentration of 100 mM and incubate at room temperature for 30 min
Volume is 10 mL, (75.07 g/mol * 0.1 mol/l * 0.01 l = 0.0751 g) Add 0.0751 g glycine

9. Centrifuge at 25 000 x g (13.000) for 30-60 min.

10. Resuspend the pellet in 50 mM PBS , gentle vortexing or bath sonicator.

11. Repeat step 9 and 10 twice.

Appendix C: Confocal settings

The settings displayed in table C1 and C2 were used to capture movies of the red (carboxyl F8810/amine F8763) and yellow-green (amine F8764) nanoparticles from Molecular Probes Invitrogen by the Leica confocal microscope TSC SP5, type DMI6000.

Table C1. Overview of settings used to capture movies of the red nanoparticles from Invitrogen.

Laser		DPSS, 561		
	power	51 %		
Beam path setting		Cy3		
PMT		PMT2		
	Mode	Leica/Cy3		
	Gain	658		
	Offset	-2 %		
Immage resolution		512x512 pixels		
Scan speed		8000 Hz		
Zoom factor		4		
Pinhole		111.44 µm		
Z-stack		Not used		
Line Average		1		
Time average		1		
Aquisation mode		xyt		
Time intervall		minimize		
Duration		20 s		
Objective		HCX PLAPO CS 63.0x1.20 WATER UV		

Table C2. Overview of settings used to capture movies of the yellow-green nanoparticles from Invitrogen.

Laser		Argon, 488		
	power	15 %		
Beam path setting		FITC		
PMT		PMT1		
	Mode	Leica/FITC		
	Gain	621		
	Offset	-2 %		
Immage resolution		512x512 pixels		
Scan speed		8000 Hz		
Zoom factor		4		
Pinhole		111.33 µm		
Z-stack		Not used		
Line Average		1		
Time average		1		
Aquisation mode		xyt		
Time intervall		minimize		
Duration		20 s		
Objective		HCX PLAPO CS 63.0x1.20 WATER UV		

Appendix D: Matlab code

The code was created by Astrid Bjørkøy, for Catherine T. Nordgård in 2011. It is used to convert all trajectory-positions into mean square displacement (MSD) values in Matlab. Input and output file to Matlab was .txt. Alterations was made from the original code concerning file source and saving positions, only to match the computer used for the work.
Matlab R2011b (7.13.0.564) was downloaded from NTNU Progdist 16.11.2011.

```
function ParticleTracker


% Prompt for lag time between frames
% Promt for name of resultfile!
prompt = {'Enter time interval:','Enter name of result file:'};
dlg_title = 'Input for Trajectory Calculations';
num_lines = 1;
def = {'1','results.txt'};
answer = inputdlg(prompt,dlg_title,num_lines,def);

timeinterval = str2double(answer{1});
filnavn = answer{2};

% Open the file with the trajectory data
[File, Path] = uigetfile('*.txt','Open Trajectory file',...
        'C:\MPT\','MultiSelect','Off')

s1 = char(strcat(Path,File));
fid = fopen(s1);

k = 1;
% Figure out what trajectories are in this file, put the names in
% Nr.Trajectory and the number of frames for particle k in Particles
while 1
   tline = fgetl(fid);
   if ~ischar(tline),   break,   end
   if ~isempty(tline)
      if tline(1) == '%'
         nr = 0;
         Nr(k).Trajectory = tline(4:end);
         k = k+1;
      else nr = nr+1;
```

```
        end
    else Particles(k-1) = nr;
    end
end
fclose(fid);

% Import the trajectory data and put data in newData1
rawData1 = importdata(s1);

% For some simple files (such as a CSV or JPEG files), IMPORTDATA might
% return a simple array.  If so, generate a structure so that the output
% matches that from the Import Wizard.
[unused,name] = fileparts(s1); %#ok
newData1.(genvarname(name)) = rawData1;

% Create new variables in the base workspace from those fields.
vars = fieldnames(newData1);
for i = 1:length(vars)
    assignin('base', vars{i}, newData1.(vars{i}));
end

j = 1;
pend = 0;

% For each particle, calculate the msd's for each time step!
% The frame number and (x,y) for each particle are between pstart and pend
% in the data file newData1.
for particle = 1:length(Particles)
    pstart = pend + 1;
    pend = pstart + (Particles(particle)-1);
    % p is an array containing the frame numbers
    p = newData1.(genvarname(name))(pstart:pend,1);
    x = newData1.(genvarname(name))(pstart:pend,2);
    y = newData1.(genvarname(name))(pstart:pend,3);
    % maxstep is the maximum lag time possible for the particle
    maxstep = p(end)-p(1);
    for step = 1:maxstep
        ave = [];  % vector of msd's
        i = p(1);  % number of startframe
        while i+step <= p(end)
            % ignore frames missing!
            if ~ismember(i,p) || ~ismember((i+step),p)
            else
                % find the correct position in p, x and y for i and i+step
                i1 = find(p==i);
                i2 = find(p==(i+step));
                new =((x(i1)-x(i2))^2 + (y(i1)-y(i2))^2);
```

```
            ave = [new ave];
        end
        i = i+1;
    end
    if ~isempty(ave)
        msd(particle, step) = mean(ave); %mean msd for this step/lag time
    end
  end
end


% Save the data to a file: lag time in first column, data for the
% particles in the other columns.
 datafile = strcat(Path, filnavn);
 fid = fopen(char(datafile),'a');

 fprintf(fid,'%s', 'Step');
 for i = 1:length(Particles)
    fprintf(fid,'\t %s',Nr(i).Trajectory);
 end
 fprintf(fid,'\n');

 % size(msd,2) is the maximum number of frames for the particles
 % in the data file newData1
 for i = 1:size(msd,2)
    fprintf(fid,'%6.4f \t', i*timeinterval);
    for j = 1:length(Particles)
        % if there's data missing for this lag time, skip info!
        % else save the result
        if msd(j,i) == 0 fprintf(fid,'\t');
        else fprintf(fid,'%6.4f \t',msd(j,i));
        end
    end
    fprintf(fid,'\n');
 end


end
```

Appendix E: Description of data analysis of MPT .lif-files

Data analysis have been a great part of the work in this thesis. All work was done on a Sony Vaio portable computer with a 32-bit operating system running Windows Vista. All programs and plugins used were downloaded from the NTNU Progdist and ImageJ homepage the autumn 2011.

The movies obtained from the Leica confocal microscope was saved as .lif-files. To open these in ImageJ the plugin *LOCI bio-formats*, was installed, and to analyze the trajectories another plugin, the *SpecleTrackerJ* was installed.

In ImageJ: Plugins →LOCI → Bio-formats importer →(View stack with: Standard ImageJ, Stack order: Default, Dataset organization: Open files individually, Color options: Autoscale)

The chosen movie is opened in ImageJ. Then choose SpeckleTrackerJ from the plugin-menu.

In SpeckleTrackerJ: Model: Diffusing spot
Select Region → Locate → Locate Speckles
Macro: Batch Locate and Track → Aquire →Set parameters (only the following two parameters was set, the rest of the parameters were accepted as suggested by the program after acquiring)

- Batch Locate Link Frames: Number of frames the program searches backwards and couple together particles disappearing/occurring close to each other. Not always correct, must be controlled. Set to 50 when looking at >200 frames.
- Batch Locate Minimum Duration: Minimum number of frames a particle must be present to be approved as a particle. Set to 5 frames.

→Batch Locate and Track.

Control the trajectories. Split/Merge if necessary. Particles may also be chosen manually and tracked by Auto Track All.

Change to adjustment model. “This model applies the center of intensity algorithm to each speckle mark. The position is updated by finding the center of intensity over a 5x5 square centered at the speckle mark. The algorithm is applied five times or until the displacement is less than 0.01 px.” – From Smith. (Smith et al., 2011)
Macros →Measure speckle track. And copy these values into a txt-file. Repeat for all trajectories. In the txt-file, name the different sets of values “%% Trajectory 1” - “%% Trajectory X”, with one line of air between each set, and two empty lines at the end, under the last trajectory. Save the txt-file in a folder with the same name and placement mentioned in line 18 in the Matlab-code, or change the code so this name corresponds to the location where the txt-file is saved.

Run the ParticleTracker.m in Matlab with time interval 0.07. Choose the saved txt-file.

Open the saved Matlab-result txt-file and replace all . (dots) with , (comma). If this step is skipped SigmaPlot will interpret all values as dates. (This step can be skipped if the settings on the computer have dots as decimal point.)

Open the file in SigmaPlot (FieldFormat: Tab delimited). Then the desired MSD-graphs may be made. All values are copied into Exel and the formula $D_{eff} = (MSD)/4\tau$ is used on all values to obtain values for D_{eff}. Then the average of all MSD values for the same τ is found, $<MSD>$, and this is used to calculate the $<D_{eff}>$. All values are copied back into SigmaPlot and the desired graphs are made.